Large-scale hydrogen production *via* water electrolysis: a techno-economic and environmental assessment

Electronic supplementary information (ESI)

Tom Terlouw[a,b*], Christian Bauer[a*], Russell McKenna[c,d], and Marco Mazzotti[b]

[a] Technology Assessment Group, Laboratory for Energy Systems Analysis, 5232 Villigen PSI, Switzerland

[b] Institute of Energy and Process Engineering, ETH Zürich, Zürich 8092, Switzerland

[c] Chair of Energy Systems Analysis, Department of Mechanical and Process Engineering, ETH Zürich, Zürich 8092, Switzerland

[d] Laboratory for Energy Systems Analysis, 5232 Villigen PSI, Switzerland

[*] *Corresponding authors. tom.terlouw@psi.ch, christian.bauer@psi.ch*

Contents

A Optimization problem

Mixed integer linear programming (MILP) is used to optimally design and operate the hydrogen production systems, since these optimization problems prove to be mathematical efficient—in terms of computational time—and they can be more complex compared to linear programming due to the introduction of integer variables.[1] In general, a MILP problem can be formulated in the following way[2]:

$$\begin{aligned} &\text{minimize}(\mathbf{c}^T\mathbf{x} + \mathbf{d}^T\mathbf{y}) \\ \\ &\text{subjected to:} \\ &A\mathbf{x} + B\mathrm{y} = \mathbf{b}, \\ &\mathbf{x} \geq 0, \in \mathbb{R}^N, \mathbf{y} \in \{0,1\}^M, \end{aligned} \tag{1}$$

where $\mathbf{c}$ is the cost vector related to continuous decision variables in $\mathbf{x}$, $\mathbf{d}$ is the cost vector associated with the binary decision variables in $\mathbf{y}$, A and B are matrices that represent the vectors coefficients, $\mathbf{b}$ is the constraint boundary vector, and N and M are the dimensions of vectors $\mathbf{x}$ and $\mathbf{y}$, respectively.

In our optimization problem, the system is optimized for each (hourly) timeslot, $t \in \mathcal{T} = \{t_0, t_0 + \Delta t, t_0 + 2\Delta t, \ldots, T\}$. We use Python v3.8 in combination with the Gurobi v9.5 solver, and set the MIP Gap to 1% to have an acceptable solution time of our optimization problem.[3] To reduce complexity, we assume perfect foresight of energy profiles as well as electricity prices. Initially, our optimization problem minimizes the total (annualized) costs ($\mathrm{C_{an}}$) with the following objective function:

$$\text{minimize} \quad \mathrm{C_{an}} = \mathrm{C_{op}} + \mathrm{C_{inv,an}} + \mathrm{C_{rep,an}} + \mathrm{C_{om}}. \tag{2}$$

Equations (3)-(6) demonstrate the underlying cost components used in the objective function in Eq. (2), considering the investments ($\mathrm{C_{inv,an}}$), operation costs ($\mathrm{C_{op}}$), fixed operation & maintenance costs ($\mathrm{C_{om}}$), and the replacements ($\mathrm{C_{rep,an}}$).

$$\mathrm{C_{op}} = C_{\mathrm{wt}} + p_{\mathrm{period,max}} C_{\mathrm{grid,p}} + \sum_{t=1}^{T=8760} (c^t_{\mathrm{da}} p^t_{\mathrm{grid,abs}} \Delta t - c^t_{\mathrm{inj}} p^t_{\mathrm{grid,inj}} \Delta t), \tag{3}$$

$$\mathrm{C_{inv,an}} = \frac{\gamma\,(1+\gamma)^{\mathrm{L}}}{(1+\gamma)^{\mathrm{L}}-1} \sum_{j=1}^{J} \mathrm{C_{inv,j}}, \tag{4}$$

$$\mathrm{C_{om}} = \sum_{j=1}^{J} \mathrm{C_{om,j}}, \tag{5}$$

$$\mathrm{C_{rep,an}} = \sum_{j=1}^{J} \frac{\gamma\,(1+\gamma)^{\mathrm{L}}}{(1+\gamma)^{\mathrm{L}}-1} \frac{\mathrm{C_{rep,j}}}{(1+\gamma)^{\mathrm{L_j}}}, \tag{6}$$

where we consider a set of system components ($\mathcal{J}$) indexed by $j \in \{1, 2, \dots, J\}$, Δt represents the timestep, γ is the discount rate [-], $p^t_{\mathrm{grid,abs}}$ is the power absorbed from the grid at t [kW], $p^t_{\mathrm{grid,inj}}$ is the power injected into the grid at t [kW], C_{wt} are the annual costs for desalination [Euro], $p_{\mathrm{period,max}}$ is a variable to determine the maximum grid absorption or injection peak reached during assessment period T [kW], $C_{\mathrm{grid,p}}$ is the specific cost for the demand charge for the grid absorption/injection peak [Euro/kW], c^t_{inj} is the remuneration received for grid electricity injection at t [Euro/kWh], c^t_{da} is the day-ahead electricity price at t [Euro/kWh], $\mathrm{L_j}$ is the replacement year of a system component j [years], $\mathrm{C_{om,j}}$ are the annual operation and maintenance costs of a system component j [Euro], $\mathrm{C_{inv,j}}$ are the investments of a system component j [Euro], $\mathrm{C_{rep,j}}$ are the replacements of a system component j [Euro].

For all system components, the costs linearly scale with the size of the component. Indeed, piecewise affine (PWA) correlations can be used to model economies of scale of capital costs in MILP.[2] However, we excluded this into our MILP problem to avoid complexity as most installed system components have a large installed capacity in our study, and therefore the expected economies of scale are expected to be minimal. Logically, grid electricity related costs are not included in the fully autonomous configuration. In the latter case, operation costs only include water desalination costs. It is worth noting that some components need (multiple) replacements during the system lifetime; we account for them with the selected methodology for replacement expenditures. For more explanation on our approach, one could follow the examples of Homer Energy in Ref.[4]. Further, replacement expenditures have been roughly assumed to be 75% of the initial investment for all technologies, to consider the re-use of system components as well as their (future) technological improvements.

As explained in the main body of the article, we introduce a second objective to minimize life cycle GHG emissions ($\mathrm{G_{an}}$), which results in a multi-objective optimization problem, considering GHG emissions from system operation ($\mathrm{G_{op}}$) as well as from the production and replacement of all system components ($\mathrm{G_{inst}}$). The ϵ-constraint method is used to solve this multi-objective problem. The Pareto fronts are generated by means of the ϵ-constraint method, which transforms the optimization problem into a single objective optimization problem—only for annualized costs—with a constraint on life cycle GHG emissions.[5,6] To do so, two single optimizations are performed first for each configuration, on annualized costs and GHG emissions, respectively. Next, the lowest and highest GHG emissions are selected from the latter simulations. After that, the difference of these two points are divided into equally sized steps, which are used as constraints in the next step. And lastly, the problem is solved as a single objective problem on annualized costs, using the set of constraints on GHG emissions from the previous step. The second objective minimizes the annual life cycle GHG emissions with Eq. (7).

$$\text{minimize} \quad \mathrm{G_{an}} = \mathrm{G_{op}} + \mathrm{G_{inst}}. \tag{7}$$

Equations (8)-(9) demonstrate the underlying components of the total GHG emissions used in the objective function of Eq. (7).

$$\mathrm{G_{op}} = 365\mathrm{g_{water}}\mathrm{N_{kg,H2}} + \sum_{t=1}^{T=8760} g^t p^t_{\text{grid,abs}}\Delta t, \tag{8}$$

$$\mathrm{G_{inst}} = \frac{\sum_{j=1}^{J} \mathrm{G_j}\frac{\mathrm{L}}{\mathrm{L_j}}}{\mathrm{L}}, \tag{9}$$

where $\mathrm{g_{water}}$ are the GHG emissions from water desalination and deionization [kg CO_2-eq./kg H_2], $\mathrm{N_{kg,H2}}$ is the daily hydrogen production rate [kg H_2], g^t are the hourly GHG emissions from the electricity grid at t [kg CO_2-eq./kWh], $\mathrm{G_j}$ are the GHG emissions generated from the construction of a system component j [kg CO_2-eq.].

Next, the constraints for each system configuration are explained.

A.1 Constraints: grid-connected

The grid-connected configuration is connected to the electricity grid, the required electricity for the electrolyzer is therefore absorbed from the grid ($p^t_{\text{grid,abs}}$), and electricity could theoretically be injected back into the electricity grid ($p^t_{\text{grid,inj}}$). First, a power balance is required to ensure a reliable operation of the hydrogen production system considering the power demand of the electrolyzer ($p^t_{\text{elect,in}}$), the compressor (p^t_{comp}), and the electricity requirement for the desalination plant (p^t_{des}).

$$p^t_{\text{elect,in}} + p^t_{\text{comp}} + p^t_{\text{des}} = (p^t_{\text{grid,abs}} - p^t_{\text{grid,inj}}), \quad \forall t. \tag{10}$$

The following constraints are required to consider the power boundaries of the cables of the electricity grid ($P_{\text{grid,max}}$), which has been set to 40 MW. It is worth noting that the latter constraint can be set stricter to avoid large grid absorption and grid injection peaks, however, this usually requires additional flexibility but reduces grid connection costs (assumed to be 180 Euro/kW). Binary variables are introduced ($y^t_{\text{grid,abs}}$ and $y^t_{\text{grid,inj}}$) to avoid simultaneous injection and absorption of grid electricity.

$$0 \leq p^t_{\text{grid,abs}} \leq y^t_{\text{grid,abs}} P_{\text{grid,max}}, \quad \forall t, \tag{11}$$

$$0 \leq p^t_{\text{grid,inj}} \leq y^t_{\text{grid,inj}} P_{\text{grid,max}}, \quad \forall t, \tag{12}$$

$$y^t_{\text{grid,abs}} + y^t_{\text{grid,inj}} \leq 1, \quad \forall t. \tag{13}$$

The maximum reached absorption and injection peak during assessment period T can be obtained with Eqs. (14–16). These constraints are active to determine the demand charge, which consists of the maximum power considering both grid absorption and grid injection power ($p_{\text{period,max}}$). It is worth noting that setting a higher demand charge cost could reduce the impact on the distribution grid, this demand charge costs can be found in the operation costs in Eq. (3) as part of the objective cost function from Eq. (2). Indeed, a commercial enterprise usually pays for the grid absorption peak; we, however, include grid injection to (potentially) charge large grid injection peaks in order to reduce impacts on the grid electricity distribution network.

$$p^t_{\text{grid,abs}} \leq p_{\text{period,max}}, \quad \forall t, \tag{14}$$

$$p^t_{\text{grid,inj}} \leq p_{\text{period,max}}, \quad \forall t, \tag{15}$$

$$p_{\text{period,max}} \geq 0. \tag{16}$$

The following constraints model the energy requirement and energy supplied by the electrolyzer. The output power of hydrogen delivered ($p^t_{\text{elect,out}}$), generated with the electrolyzer, can be determined for each timeslot using the input power demand ($p^t_{\text{elect,in}}$) and the efficiency of the electrolyzer (η_{elect}). Further, Eq. (18) ensures that the power demand of the electrolyzer is within the power ranges considering the capacity of the electrolyzer (cap_{elect}). For simplicity, the electrolyzer efficiency under part-load ratios and other system dynamics are not considered within our optimization problem. The argumentation and more discussion regarding this choice is provided in Section A.4.

$$p^t_{\text{elect,out}} = p^t_{\text{elect,in}} \eta_{\text{elect}}, \quad \forall t, \tag{17}$$

$$0 \leq p^t_{\text{elect,in}} \leq cap_{\text{elect}}, \quad \forall t. \tag{18}$$

The following constraint is introduced to ensure a daily hydrogen production rate of 10 tonnes ($\mathrm{N_{kg,H2}}$).

$$\sum_{t=d}^{d+24} p_{\text{elect,out}}^{t} \Delta t = \frac{\mathrm{N_{kg,H2}} \mathrm{H_{2,LHV}}}{3.6}, \quad \forall d \in \mathcal{D}, \tag{19}$$

where d is an index for the start of the days in the simulation period, $d \in \{0, 24, 48, \ldots, D\}$, $\mathrm{H_{2,LHV}}$ is the energy content of hydrogen using the lower heating value (LHV, 120 MJ per kg H_2) [MJ/kg] and 3.6 is a conversion factor [MJ/kWh]. And lastly, the following constraints are introduced to model the electricity requirement of the compressor and the desalination plant. For simplicity, it is assumed that the compressor and desalination plant follow the hydrogen production schedule of the electrolyzer.

$$p_{\text{comp}}^{t} = \frac{3.6 P_{\text{comp,h2}} p_{\text{elect,out}}^{t}}{\mathrm{H_{2,LHV}}}, \quad \forall t, \tag{20}$$

$$0 \leq p_{\text{comp}}^{t} \leq cap_{\text{comp}}, \quad \forall t, \tag{21}$$

$$p_{\text{des}}^{t} = \frac{3.6 P_{\text{des,h2}} p_{\text{elect,out}}^{t}}{\mathrm{H_{2,LHV}}}, \quad \forall t, \tag{22}$$

$$0 \leq p_{\text{des}}^{t} \leq cap_{\text{des}}, \quad \forall t, \tag{23}$$

where $P_{\text{comp,h2}}$ is the amount of energy required to compress one kilogram of hydrogen [kWh/kg], cap_{comp} is the compressor size [kWh], $P_{\text{des,h2}}$ is the amount of energy required for the desalination plant [kWh/kg] and cap_{des} is the size of desalination plant [kW].

A.2 Constraints: hybrid

The hybrid configuration is coupled to the electricity grid and can be coupled to renewable energy generators. It is worth noting that all constraint are presented for this configuration, although only new and modified constraints—compared to the previous configuration—are explained.

PV solar (p_{pv}^{t}), onshore wind ($p_{\text{wind,on}}^{t}$), and offshore wind ($p_{\text{wind,off}}^{t}$) electricity sources can be installed in the hybrid configuration. Therefore, the power supply of these energy sources are added to the power balance.

$$p_{\text{elect,in}}^{t} + p_{\text{comp}}^{t} + p_{\text{des}}^{t} = p_{\text{wind,on}}^{t} + p_{\text{wind,off}}^{t} + p_{\text{pv}}^{t} + (p_{\text{grid,abs}}^{t} - p_{\text{grid,inj}}^{t}), \quad \forall t. \tag{24}$$

The power delivered from solar PV, onshore wind, and offshore wind rely on the capacity installed of these renewable electricity sources, which are the decision variables denoted by cap_{pv}, $cap_{\text{wind,on}}$, and $cap_{\text{wind,off}}$, respectively. The pre-modelled generation profiles of PV, onshore wind, and offshore wind (per

kW_p) are denoted by P^t_{pv}, $P^t_{\text{wind,on}}$, and $P^t_{\text{wind,off}}$, respectively.

$$p^t_{\text{pv}} = P^t_{\text{pv}} cap_{\text{pv}}, \quad \forall t, \tag{25}$$

$$p^t_{\text{wind,on}} = P^t_{\text{wind,on}} cap_{\text{wind,on}}, \quad \forall t, \tag{26}$$

$$p^t_{\text{wind,off}} = P^t_{\text{wind,off}} cap_{\text{wind,off}}, \quad \forall t, \tag{27}$$

$$cap_{\text{pv}}, cap_{\text{wind,on}}, cap_{\text{wind,off}} \geq 0. \tag{28}$$

Further, onshore wind and ground-mounted PV capacity can be limited by the amount of land area available on an island. The following constraints are introduced to consider the maximum amount of PV capacity ($C_{\text{pv,max}}$) and onshore wind capacity ($C_{\text{wind,on,max}}$), which can be installed on an island considering island-specific boundary conditions. The maximum capacities for onshore wind are provided in the main body of the article. For the maximum amount of solar PV capacity installed, we assume that a maximum of 15% of the total land area of the island is available for ground-mounted PV systems. An additional 5% (on top of the initial 10%) is considered, since solar panels might also be installed on water as floating PV panels in the future.

$$cap_{\text{pv}} \leq C_{\text{pv,max}}, \tag{29}$$

$$cap_{\text{wind,on}} \leq C_{\text{wind,on,max}}. \tag{30}$$

And finally, the following constraints are active, which are identical compared to the previous configuration:

$$0 \leq p^t_{\text{grid,abs}} \leq y^t_{\text{grid,abs}} P_{\text{grid,max}}, \quad \forall t, \tag{31}$$

$$0 \leq p^t_{\text{grid,inj}} \leq y^t_{\text{grid,inj}} P_{\text{grid,max}}, \quad \forall t, \tag{32}$$

$$y^t_{\text{grid,abs}} + y^t_{\text{grid,inj}} \leq 1, \quad \forall t, \tag{33}$$

$$p^t_{\text{grid,abs}} \leq p_{\text{period,max}}, \quad \forall t, \tag{34}$$

$$p^t_{\text{grid,inj}} \leq p_{\text{period,max}}, \quad \forall t, \tag{35}$$

$$p_{\text{period,max}} \geq 0, \tag{36}$$

$$p^t_{\text{elect,out}} = p^t_{\text{elect,in}} \eta_{\text{elect}}, \quad \forall t, \tag{37}$$

$$0 \leq p^t_{\text{elect,in}} \leq cap_{\text{elect}}, \quad \forall t, \tag{38}$$

$$\sum_{t=d}^{d+\mathtt{D}} p^t_{\text{elect,out}} \Delta t = \frac{\mathrm{N}_{\text{kg,H2}} \mathrm{H}_{2,\text{LHV}}}{3.6}, \quad \forall d \in \mathcal{D}, \tag{39}$$

$$p^t_{\text{comp}} = \frac{3.6 P_{\text{comp,h2}} p^t_{\text{elect,out}}}{\mathrm{H}_{2,\text{LHV}}}, \quad \forall t, \tag{40}$$

$$0 \leq p^t_{\text{comp}} \leq cap_{\text{comp}}, \quad \forall t, \tag{41}$$

$$p^t_{\text{des}} = \frac{3.6 P_{\text{des,h2}} p^t_{\text{elect,out}}}{\mathrm{H}_{2,\text{LHV}}}, \quad \forall t, \tag{42}$$

$$0 \leq p^t_{\text{des}} \leq cap_{\text{des}}, \quad \forall t. \tag{43}$$

Constraints: hybrid - green

As explained in the main body of the article, the *hybrid - green* sub-configuration is introduced to ensure a hybrid configuration with low-carbon GHG emissions to comply with the standards of green hydrogen of CertifHy; a specific carbon intensity of hydrogen equal to or lower than 4.4 kg CO_2-eq. per kg H_2 ($\mathrm{G}_{\text{green,h2}}$).[7] All constraints are adopted as explained in the previous section. The difference between the previous configuration is that a constraint is introduced on the annual GHG emissions objective ("365" represents 365 days during one year).

$$\mathrm{G}_{\text{an}} \leq 365 \mathrm{G}_{\text{green,h2}} \mathrm{N}_{\text{kg,H2}}. \tag{44}$$

We perform a minimization on annual GHG emissions when this GHG emissions requirement cannot be reached, which could for example happen in geographical locations with insufficient and discontinued supply of renewable electricity sources. Consequently, this could lead to tremendous oversizing of system components and therefore additional environmental burdens and costs.

A.3 Constraints: autonomous

The autonomous configuration is disconnected from the electricity grid, and a battery can be installed to add flexibility to this configuration. Further, we assume that the hydrogen storage vessels have a storage capacity of five days to ensure additional flexibility. It is worth noting that Eq. (19) is slightly modified with Eq. (62) to achieve the latter goal and that the hydrogen storage volume is five times bigger. The power balance includes power supply from renewable electricity generators and from discharging the battery ($p^t_{\text{bat,dis}}$). Power is consumed by charging the battery ($p^t_{\text{bat,ch}}$), the electrolyzer, the desalination plant, and the compressor.

$$p^t_{\text{elect,in}}+p^t_{\text{comp}} + p^t_{\text{des}} = p^t_{\text{wind,on}} + p^t_{\text{wind,off}} + p^t_{\text{pv}} + (p^t_{\text{bat,dis}} - p^t_{\text{bat,ch}}), \quad \forall t. \tag{45}$$

PV solar and wind electricity generation usually have substantial hourly, daily, and seasonal fluctuations. We therefore add the possibility to curtail renewable electricity in order to ensure the power balance. This is modelled using inequality constraints instead of equality constraints.

$$p^t_{\text{pv}} \leq P^t_{\text{pv}} cap_{\text{pv}}, \quad \forall t, \tag{46}$$

$$p^t_{\text{wind,on}} \leq P^t_{\text{wind,on}} cap_{\text{wind,on}}, \quad \forall t, \tag{47}$$

$$p^t_{\text{wind,off}} \leq P^t_{\text{wind,off}} cap_{\text{wind,off}}, \quad \forall t, \tag{48}$$

$$cap_{\text{pv}}, cap_{\text{wind,on}}, cap_{\text{wind,off}} \geq 0. \tag{49}$$

Further, the amount of curtailed PV ($p^t_{\text{pv,curt}}$), onshore wind electricity ($p^t_{\text{wind,curt,on}}$), and offshore wind ($p^t_{\text{wind,curt,off}}$) can be determined with the following constraints. It is worth noting that this is the difference between the PV and wind which might be generated (without curtailment), and the actual PV and wind power delivered.

$$p^t_{\text{pv,curt}} = P^t_{\text{pv}} cap_{\text{pv}} - p^t_{\text{pv}}, \quad \forall t, \tag{50}$$

$$p^t_{\text{wind,curt,on}} = P^t_{\text{wind,on}} cap_{\text{wind,on}} - p^t_{\text{wind,on}}, \forall t, \tag{51}$$

$$p^t_{\text{wind,curt,off}} = P^t_{\text{wind,off}} cap_{\text{wind,off}} - p^t_{\text{wind,off}}, \quad \forall t. \tag{52}$$

A battery can be introduced to add flexibility to the autonomous configuration. The battery energy capacity ($cap_{\text{e,bat}}$) and power capacity ($cap_{\text{p,bat}}$) are introduced as decision variables in our optimization problem to optimally design the battery system.

The battery energy storage dynamics (e^t_{bat}) contains of battery charging and discharging considering a charging ($\eta_{\text{bat,ch}}$) and discharging efficiency ($\eta_{\text{bat,dis}}$) which are assumed to be equal. Further, a self-discharging factor of the battery has been considered (s_{dis}).[8,9]

$$e^t_{\text{bat}} = e^{t-1}_{\text{bat}}(1 - s_{\text{dis}}\Delta t)+\eta_{\text{ch}}p^t_{\text{bat,ch}}\Delta t - \frac{p^t_{\text{bat,dis}}\Delta t}{\eta_{\text{dis}}}, \ \ \forall t. \tag{53}$$

Binary variables are introduced to prevent simultaneous charging ($y^t_{\text{bat,ch}}$) and discharging ($y^t_{\text{bat,dis}}$) of the battery.

$$y^t_{\text{bat,ch}} + y^t_{\text{bat,dis}} \leq 1 \ \ \forall t. \tag{54}$$

Indeed, the introduction of these binary variables multiplied with the battery power capacity—required to avoid simultaneous charging and discharging—results in bilinear terms (*i.e.*, $y^t_{\text{bat,ch}}cap_{\text{p,bat}}$ and $y^t_{\text{bat,dis}}cap_{\text{p,bat}}$):

$$0 \leq p^t_{\text{bat,ch}} \leq y^t_{\text{bat,ch}}cap_{\text{p,bat}}, \ \ \forall t, \tag{55}$$

$$0 \leq p^t_{\text{bat,dis}} \leq y^t_{\text{bat,dis}}cap_{\text{p,bat}}, \ \ \forall t. \tag{56}$$

It is worth noting that such a bilinear term can be linearized with the introduction of an auxiliary variable: $\widetilde{p}^t_{\text{ch,aux}}$.[10] To do so, the following constraints are introduced to linearize the bi-linear term $y^t_{\text{bat,ch}}cap_{\text{p,bat}}$. Further, we set $\underline{P}$ to zero and $\overline{P}$ to a large number (in this paper 5E5).

$$\underline{P}y^t_{\text{bat,ch}} \leq \widetilde{p}^t_{\text{ch,aux}} \leq \overline{P}y^t_{\text{bat,ch}}, \ \ \forall t, \tag{57}$$

$$cap_{\text{p,bat}} - \overline{P}(1 - y^t_{\text{bat,ch}}) \leq \widetilde{p}^t_{\text{ch,aux}} \leq cap_{\text{p,bat}}, \ \ \forall t. \tag{58}$$

Further, we introduce another auxiliary variable also for battery discharging ($\widetilde{p}^t_{\text{dis,aux}}$) to linearize the bilinear term in Eq. (56). We apply the same approach as described with Eqs. (57)–(58), but now for battery discharging.

We assume that maximum battery energy capacity ($C_{\text{bat,max}}$) installed is constrained to 500 MWh, to prevent unrealistically large battery systems. Further, the amount of energy stored in the battery must meet the minimum (SoC_{min}) and maximum state of charge (SoC_{max}). This is needed to prevent tremendous battery degradation rates.[11,12]

$$\text{SoC}_{\text{min}}cap_{\text{e,bat}} \leq e^t_{\text{bat}} \leq \text{SoC}_{\text{max}}cap_{\text{e,bat}}, \ \ \forall t, \tag{59}$$

$$cap_{\text{e,bat}} \leq C_{\text{bat,max}}, \tag{60}$$

$$cap_{\text{e,bat}}, cap_{\text{p,bat}} \geq 0. \tag{61}$$

The following constraint is introduced to ensure a hydrogen production rate of 50 tonnes in 5 days (120 hours), *i.e.*, on average 10 tonnes hydrogen production per day.

$$\sum_{t=w}^{w+\mathtt{W}} p^t_{\text{elect,out}} \Delta t = \frac{5\mathrm{N}_{\text{kg,H2}}\mathrm{H}_{2,\text{LHV}}}{3.6}, \quad \forall w \in \mathcal{W}, \tag{62}$$

where w is an index for the start of the chosen time interval to meet the production requirement in the simulation period, $w \in \{0, 120, 240, \ldots, W\}$, $\mathtt{W}$ represents 120 hours corresponding to five days [hours].

And finally, the following constraints are introduced, these are identical compared to the previous configurations:

$$cap_{\text{pv}} \leq C_{\text{pv,max}}, \tag{63}$$

$$cap_{\text{wind,on}} \leq C_{\text{wind,on,max}}, \tag{64}$$

$$p^t_{\text{elect,out}} = p^t_{\text{elect,in}} \eta_{\text{elect}}, \quad \forall t, \tag{65}$$

$$0 \leq p^t_{\text{elect,in}} \leq cap_{\text{elect}}, \quad \forall t, \tag{66}$$

$$p^t_{\text{comp}} = \frac{3.6 P_{\text{comp,h2}} p^t_{\text{elect,out}}}{\mathrm{H}_{2,\text{LHV}}}, \quad \forall t, \tag{67}$$

$$0 \leq p^t_{\text{comp}} \leq cap_{\text{comp}}, \quad \forall t, \tag{68}$$

$$p^t_{\text{des}} = \frac{3.6 P_{\text{des,h2}} p^t_{\text{elect,out}}}{\mathrm{H}_{2,\text{LHV}}}, \quad \forall t, \tag{69}$$

$$0 \leq p^t_{\text{des}} \leq cap_{\text{des}}, \quad \forall t. \tag{70}$$

Constraints: autonomous - grid injection

As explained in the main body of the article, the *autonomous - grid injection* sub-configuration is introduced to consider revenue from excess renewable electricity generation, and to avoid tremendous amounts of curtailment of PV and wind electricity generation. All constraints are adopted as explained in the previous section. Only modifications and new constraints are explained compared to Section A.3.

Constraint (45) is modified to consider the possibility of grid electricity injection.

$$p^t_{\text{elect,in}} + p^t_{\text{comp}} + p^t_{\text{des}} = p^t_{\text{wind,on}} + p^t_{\text{wind,off}} + p^t_{\text{pv}} + (p^t_{\text{bat,dis}} - p^t_{\text{bat,ch}}) - p^t_{\text{grid,inj}}, \quad \forall t. \tag{71}$$

Further, the following constraint are introduced to consider the power boundaries of the electricity grid and to determine the demand charge.

$$0 \leq p^t_{\text{grid,inj}} \leq P_{\text{grid,max}}, \quad \forall t, \tag{72}$$

$$p^t_{\text{grid,inj}} \leq p_{\text{period,max}}, \quad \forall t, \tag{73}$$

$$p_{\text{period,max}} \geq 0. \tag{74}$$

A.4 Optimization problem: discussion

More detailed system optimization could be performed with a higher temporal resolution of for example 15 minutes or 1 minute. This should consider additional constraints associated to the electrolyzer to consider ramp-up and ramp-down rates as well as minimum down-times and different efficiencies under part-load operation.[13,14] It is, however, worth noting that PEM electrolyzer are flexible considering the latter considerations, since the ramp-up and ramp-down times are in the order of 10 minutes and thus much smaller than the hourly resolution of our optimization algorithm.[14] Further, our simplified assumption of a constant conversion efficiency of the PEM electrolyzer is supposed to exhibit only small discrepancies compared to a more thorough analysis using different efficiencies under part-load ratios.[14] Therefore, our approach—with limited complexity of our optimization problems and therefore a reduction of the computational effort—can be considered as sufficiently accurate to assess multiple hydrogen production configurations as well as to explore a variety of renewable energy generation profiles.

The integration of such detailed constraints is, however, might be required for less flexible energy conversion technologies as well as to include a larger set of technologies, for example with the design of multi-energy systems.[2,14] Indeed, the sizing of hydrogen storage could also be included in the optimization. However, we decided to avoid additional complexity of the optimization problem, and therefore sized the storage medium in a static way. It is worth mentioning that battery and electrolyzer degradation, which depend on the operational profiles, are not considered in our analysis to reduce complexity and computational complexity of our optimization problems. On the one hand, the degradation of system components can reduce the performance and therefore could increase system costs and environmental impacts.[12,13,15,16] On the other hand, we used conservative cost numbers and lifetimes for the electrolyzer and the battery system. The integration of component degradation in the optimization problem is, however, an interesting area for future work, although this could lead to additional model complexity and a substantial computational burden as a result of the introduction of a larger set of binary variables.[14]

Table A1: LCI of all system components and grid electricity.

Sub-component	Name	Reference product	Location	Unit	Database or source
Photovoltaic system & inverter	570 kWp open ground installation, multi-Si, on open ground	570 kWp open ground installation, multi-Si, on open ground	RER	unit	[19]
Onshore Wind turbines	wind turbine construction, 2MW, onshore & market for network connection, turbine 2MW, onshore	wind turbine, 2MW, onshore & wind turbine network connection, 2MW, onshore	GLO	unit	[20]
Offshore Wind turbines	market for wind power plant, 2MW, offshore, fixed parts & market for wind power plant, 2MW, offshore, moving parts	wind power plant, 2MW, offshore, fixed parts & wind power plant, 2MW, offshore, moving parts	GLO	unit	[20]
Compressor	market for air compressor, screw-type compressor, 300kW	air compressor, screw-type compressor, 300kW	GLO	unit	[20]
Hydrogen storage	hydrogen storage, vessel	hydrogen storage, vessel	RER	unit	[18]
Battery; Li-ion (NMC)	Li-ion (NMC)	Li-ion (NMC)	GLO	kilowatt hour	[12,21]
Battery; Battery management system	Battery management system, kWh	Battery management system, kWh	GLO	kilowatt hour	[12,21]
Battery; Energy management system	Energy management system, kWh	Energy management system, kWh	GLO	kilowatt hour	[12,21]
Power conditioning system, container system	Power conditioning system, container system	Power conditioning system, container system	GLO	kW	[12,21]
Electrolyzer (PEM, 1 MW unit)	electrolyzer, PEM	electrolyzer, PEM	GLO	unit	[17]
Deionization of water	water production, deionised [modified, see text]	water, deionised	Europe without Switzerland	kilogram	Adapted, based on[20]
Reverse osmosis in desalination plant	tap water production, seawater reverse osmosis, ultrafiltration pretreatment, baseline module, single stage [modified, see text]	tap water	GLO	kilogram	Adapted, based on[20]
Grid electricity: Crete	market for electricity, low voltage	electricity, low voltage	GR	kilowatt hour	[20]
Grid electricity: Eigerøy	market for electricity, low voltage	electricity, low voltage	NO	kilowatt hour	[20]
Grid electricity: Western isles	market for electricity, low voltage	electricity, low voltage	GB	kilowatt hour	[20]
Grid electricity: Tenerife	market for electricity, low voltage	electricity, low voltage	ES	kilowatt hour	[20]
Grid electricity: Borkum	market for electricity, low voltage	electricity, low voltage	DE	kilowatt hour	[20]

B Life cycle inventory

This chapter provides the life cycle inventory for foreground processes used in our environmental life cycle analysis. The specific datasets are provided with the life cycle inventory name, location, reference product, and database or literature source in Table A1. It is worth noting that not all of these sub-components are installed for each configuration. The activity regarding reverse osmosis has been modified—"tap water production, seawater reverse osmosis.."—since electricity consumption has been removed from this activity. The reason is that the electricity consumption needed for the desalination plant has been added to the optimization problem in order to use the location-specific electricity source as defined in the optimization problem, which can for example be provided by grid electricity, PV, or wind electricity. Further, the activity regarding the deionization of water has been modified—"water production, deionised"—to avoid double counting; since we assume these water flows derive from sea water with the previous modified activity. We therefore delete the water biosphere flows.

The life cycle inventory of the polymer electrolyte membrane (PEM) electrolyzer has been generated based on the data provided in Bareiß *et al.* [17] and is provided in Table A2. Further, the inventory of the storage vessel is based on the work of Palmer *et al.* [18], and has also been provided in the latter table.

Table A2: LCI of the PEM[17] electrolyzer and the hydrogen storage vessels.[18]

hydrogen storage, vessel			unit		RER	
Name	**Reference Product**	**Amount**	**Unit**	**Categories**	**Location**	**Type**
Occupation, industrial area		9.60E+02	square meter-year	natural resource:land		biosphere
Transformation, from grassland, natural (non-use)		4.80E+01	square meter	natural resource:land		biosphere
Transformation, to industrial area		4.80E+01	square meter	natural resource:land		biosphere
hydrogen storage, vessel	hydrogen storage, vessel	1.00E+00	unit		RER	production
market for scrap steel	scrap steel	-8.19E+04	kilogram		RoW	technosphere
steel production, chromium steel 18/8, hot rolled	steel, chromium steel 18/8, hot rolled	1.26E+05	kilogram		RER	technosphere
treatment of waste reinforcement steel, recycling	waste reinforcement steel	-4.41E+04	kilogram		RoW	technosphere

electrolyzer, PEM			unit		GLO	
Name	**Reference Product**	**Amount**	**Unit**	**Categories**	**Location**	**Type**
electrolyzer, PEM	electrolyzer, PEM	1.00E+00	unit		GLO	production
electrolyzer, PEM, Balance of Plant	electrolyzer, PEM, Balance of Plant	3.50E-01	unit		GLO	technosphere
electrolyzer, PEM, Stack	electrolyzer, PEM, Stack	1.00E+00	unit		GLO	technosphere

electrolyzer, PEM, near future			unit		GLO	
Name	**Reference Product**	**Amount**	**Unit**	**Categories**	**Location**	**Type**
electrolyzer, PEM, Balance of Plant	electrolyzer, PEM, Balance of Plant	5.00E-01	unit		GLO	technosphere
electrolyzer, PEM, Stack, near future	electrolyzer, PEM, Stack, near future	1.00E+00	unit		GLO	technosphere
electrolyzer, PEM, near future	electrolyzer, PEM, near future	1.00E+00	unit		GLO	production

electrolyzer, PEM, Stack			unit		GLO	
Name	**Reference Product**	**Amount**	**Unit**	**Categories**	**Location**	**Type**
Iridium, in ground		7.50E-01	kilogram	natural resource:in ground		biosphere
electrolyzer, PEM, Stack	electrolyzer, PEM, Stack	1.00E+00	unit		GLO	production
market for aluminium, wrought alloy	aluminium, wrought alloy	2.70E+01	kilogram		GLO	technosphere
market for activated carbon, granular	activated carbon, granular	9.00E+00	kilogram		GLO	technosphere
market for copper, anode	copper, anode	4.50E+00	kilogram		GLO	technosphere
market for platinum	platinum	7.50E-02	kilogram		GLO	technosphere
market for steel, chromium steel 18/8, hot rolled	steel, chromium steel 18/8, hot rolled	1.00E+02	kilogram		GLO	technosphere
market for sulfuric acid	sulfuric acid	2.80E+00	kilogram		RoW	technosphere
market for tetrafluoroethylene	tetrafluoroethylene	1.32E+01	kilogram		GLO	technosphere
market for titanium, primary	titanium, primary	5.28E+02	kilogram		GLO	technosphere

electrolyzer, PEM, Stack, near future			unit		GLO	
Name	**Reference Product**	**Amount**	**Unit**	**Categories**	**Location**	**Type**
Iridium, in ground		3.70E-02	kilogram	natural resource:in ground		biosphere
electrolyzer, PEM, Stack, near future	electrolyzer, PEM, Stack, near future	1.00E+00	unit		GLO	production
market for aluminium, wrought alloy	aluminium, wrought alloy	5.40E+01	kilogram		GLO	technosphere
market for activated carbon, granular	activated carbon, granular	4.50E+00	kilogram		GLO	technosphere
market for copper, anode	copper, anode	9.00E+00	kilogram		GLO	technosphere
market for platinum	platinum	1.00E-02	kilogram		GLO	technosphere
market for steel, chromium steel 18/8, hot rolled	steel, chromium steel 18/8, hot rolled	4.00E+01	kilogram		GLO	technosphere
market for sulfuric acid	sulfuric acid	3.50E-01	kilogram		RoW	technosphere
market for tetrafluoroethylene	tetrafluoroethylene	1.65E+00	kilogram		GLO	technosphere
market for titanium, primary	titanium, primary	3.70E+01	kilogram		GLO	technosphere

electrolyzer, PEM, Balance of Plant			unit		GLO	
Name	**Reference Product**	**Amount**	**Unit**	**Categories**	**Location**	**Type**
Occupation, industrial area		2.97E+02	square meter-year	natural resource:land		biosphere
Transformation, from grassland, natural (non-use)		1.49E+01	square meter	natural resource:land		biosphere
Transformation, to industrial area		1.49E+01	square meter	natural resource:land		biosphere
electrolyzer, PEM, Balance of Plant	electrolyzer, PEM, Balance of Plant	1.00E+00	unit		GLO	production
market for aluminium, wrought alloy	aluminium, wrought alloy	1.00E+02	kilogram		GLO	technosphere
market for chemical, organic	chemical, organic	2.00E+02	kilogram		GLO	technosphere
market for copper, anode	copper, anode	1.00E+02	kilogram		GLO	technosphere
market for electronics, for control units	electronics, for control units	1.10E+03	kilogram		GLO	technosphere
market for polypropylene, granulate	polypropylene, granulate	3.00E+02	kilogram		GLO	technosphere
market for steel, chromium steel 18/8	steel, chromium steel 18/8	1.90E+03	kilogram		GLO	technosphere
market for steel, low-alloyed	steel, low-alloyed	4.80E+03	kilogram		GLO	technosphere
market group for concrete, normal	concrete, normal	2.33E+00	cubic meter		GLO	technosphere

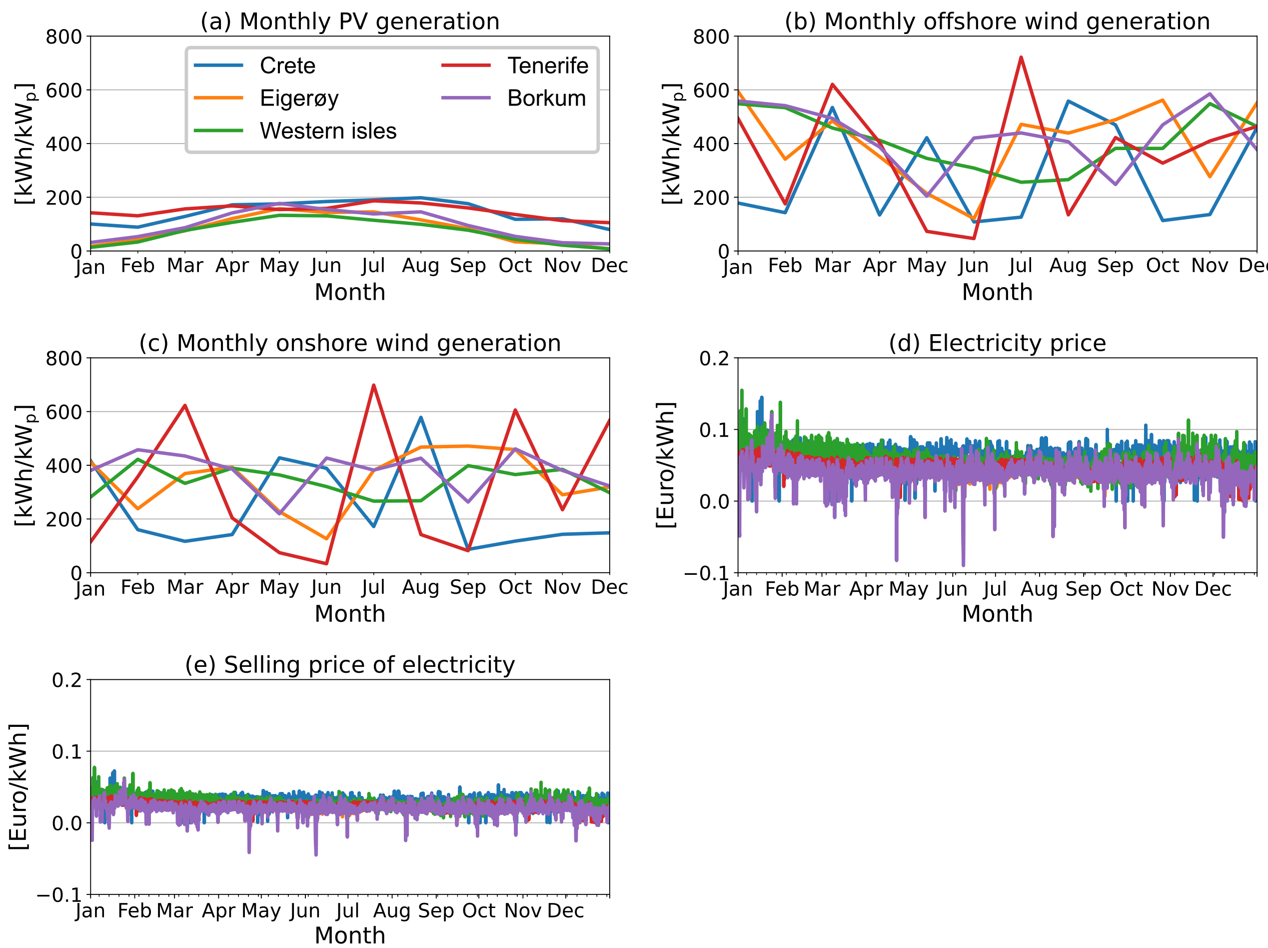

Figure A1: The first three subplots illustrate annual PV, offshore wind, and onshore wind generation profiles aggregated on a monthly basis on the selection of geographical islands per kW_p capacity installed. The fourth and fifth subplot visualize the hourly grid electricity prices and selling price of electricity to the electricity network for assessment year 2019-2020.

C PV and wind generation profiles

The main hourly data used for our five different case studies is visualized in Figure A1. The PV and wind electricity generation profiles are presented on the top left and the top right subplot, respectively. These subplots show the monthly summed PV generation and wind generation per geographical location. It is worth noting that all geographical locations have very different PV and wind generation profiles. For example, Crete and Tenerife have substantial and rather stable solar PV output during the entire year, while the PV solar seasonality in Borkum, Western Isles, and Eigerøy is more pronounced resulting in lower accumulated PV output over the entire year. The monthly wind electricity demonstrates a different view; Western Isles, Borkum, and Eigerøy show a comparably high wind energy supply during the entire year, while Tenerife and

Table A3: Longitude and Latitude of selected case studies.

	Country	PV and onshore		offshore	
		Latitude	**Longitude**	**Latitude**	**Longitude**
Crete	Greece	35.31	25.21	35.34	25.15
Eigerøy	Norway	58.45	5.97	58.44	5.86
Western Isles	United Kingdom	58.38	-6.52	58.38	-6.53
Tenerife	Spain	28.07	-16.71	28.04	-16.71
Borkum	Germany	53.58	6.70	53.59	6.74

Crete show very variable as well as lower wind energy output during the year.

The national day-ahead electricity prices from the electricity grid are provided in the fourth subplot. Electricity prices are generally the lowest in Borkum (Germany), even reaching negative electricity prices during some hourly time intervals. The electricity prices in Crete (Greece) are the highest within our case studies.

Further, specific geographical information of the selected case studies—regarding latitude and longitude—is provided in Table A3. It is worth noting that the chosen geographical location for the PV system and onshore wind slightly differ compared to the location of offshore wind. The PV and onshore wind location are chosen such that the location is on the mainland, while the location of offshore wind is at the coastal zone of a location (since the typical meteorological year (TMY) function of PVGIS does not provide data for offshore locations). For the generation of wind profiles, we set the roughness length of 0.15 for onshore locations and 0.05 for offshore/coastal locations. In reality, the roughness length of coastal/offshore locations is (much) lower, however, we are unable to obtain TMY weather data for offshore locations from PVGIS, and therefore we set the roughness length comparably high to obtain higher wind capacity factors compared to onshore wind.

D Explanation of sensitivity analysis

D.1 Future hydrogen production in 2040

A prospective analysis is performed on large-scale hydrogen production *via* water electrolysis for a (possible) future situation in year 2040, see Section 3.3.4 of the manuscript. Logically, the optimistic scenario considers the lowest costs, highest component lifetimes, and lowest discount rate (as this is usually beneficial for renewable energy technologies). These three cost scenarios are coupled to technology performance scenarios, which are based on a modification of the background LCA database. To do so, we use the open-source Python package *premise*.[22] The following future scenarios, which are based on integrated assessment models and are available in *premise* v0.4.4, are considered within our prospective analysis; representative concentration pathway (RCP) 6.0 W/m^2 (pessimistic), RCP 2.4 W/m^2 (average) and 1.9 W/m^2 (optimistic). The RCP 6.0 W/m^2, RCP 2.4 W/m^2, and 1.9 W/m^2 represent a business as usual scenario, and two more ambitious climate scenarios to maintain the global temperature increase well below 2°C, respectively.

Further, we modify the LCA foreground data for the battery system and the electrolyzer to consider technological improvements of the battery and electrolyzer industry. The latter two system components turned out to be decisive in the analysis of environmental burdens other than GHG emissions, see Sections 3 and 4 (Results and Discussion) in the main body of the article. To do so, the "near-future" LCI scenario for a PEM electrolyzer is adopted from Bareiß *et al.*[17] and the gravimetric energy density regarding the LCI of the battery pack is updated from 126 Wh kg^{-1} to 210 Wh kg^{-1}.[21,23]

D.2 Sensitivity: weather data inputs

The main environmental and economic results are first quantified based on one year of system operation using typical meteorological years (TMYs) to reduce computational efforts and data requirements. The renewable energy generation profiles used are valid for a TMY varying from 2007 to 2016. Weather data can, however, differ significantly between assessment years resulting in a different capacity factor for renewable energy generators. This leads to differences compared to an actual analysis using the entire set of lifetime years. We therefore perform a sensitivity analysis (see Section 3.3.3 of the manuscript) using weather profiles—resulting in different PV and wind generation profiles—from year 2007 until year 2016 to test the reliability and the robustness of our results when optimizing the system design for other years than a TMY. Year 2019 has been set as reference year for grid electricity prices during all assessment years.

E Explanation on data sources

E.1 Data: electricity prices, wind and PV generation data

National day-ahead grid electricity prices are used for grid-connected configurations using 2019 as reference year.[24] It is worth to point out that Crete (Greece) and Tenerife (Spain) have a local electricity grid and that generation mixes and electricity grid prices therefore might differ compared to the mainland.[25] Crete will, however, connect their electricity network to the national electricity grid in the coming years.[26] Further, electricity tariffs in Tenerife are subsidized to obtain similar electricity price tariffs compared to the mainland.[27] For simplicity and due to data limitations, we assume that the grid electricity prices of the latter islands are the same as the national mainland. We assume that the grid electricity injection costs, or feed-in tariff, is half of the hourly grid electricity costs.

It is worth noting that the electricity bill of electricity consumers usually includes an energy charge and a demand charge. Energy charges are considered with day-ahead electricity prices. Demand charges are assumed to be generic and are estimated on 7 Euro kW^{-1} grid peak annually,[28] since they are usually very case-specific and depend on factors such as installed capacity, the country, and geographic location. They are therefore difficult to determine for the considered locations.

Further, new grid connections usually require grid extension services. Typically a fee applies for the new grid connection, depending on the country-specific policy as well as the case-specific situation, such as the requirement and the size of the grid extension.[29] For simplicity and complexity of case-specific fees, we apply a standard grid extension fee of 180 Euro/kW grid power capacity for all grid-connected case studies considering a lifetime of 30 years.[20,28]

Weather data for the generation of the PV profiles are obtained from PVGIS.[30] TMYs are used for the reference PV profile, and therefore the temperature, wind speed, direct normal irradiation, global horizontal irradiance, and diffuse horizontal irradiance are obtained considering the last available decade. The Python package *pvlib* is used to calculate the PV generation profiles using TMY weather conditions for a specific location for open-rack ground mounted multi-Si PV installations.[31,32] The same meteorological data is used from PVGIS to calculate wind electricity profiles based on TMYs.[30] To do so, Python library *windpowerlib* has been used to calculate the wind power output of an Enercon (E126) 4.2MW turbine and a Vestas (V90/2000) 2MW turbine for offshore and onshore wind, respectively.[33]

However, insufficient weather data is available from PVGIS to calculate wind profiles other than the TMY. Therefore, weather data from meteostat has been used using the *meteostat* Python library for years other than TMY for wind profiles, *i.e.*, for the sensitivity analysis in Section D.2.[34]

Table A4: Techno-economic parameters used in our analysis for year 2020, considering a pessimistic and optimistic scenario in addition to provide error bars for Figure 1 in the main body of the manuscript. References are provided in the main body of the article.

Parameter	Pessimistic	Baseline	Optimistic	Unit
Electrolyzer				
Efficiency	0.58	0.61	0.64	[-]
Stack Lifetime	6.65	7	7.35	[years]
CAPEX	1113	1060	1007	[Euro/kW]
O&M	2	2	2	[%]
Balance of system	45	45	45	[Euro/kW]
H_2 storage				
Lifetime	19	20	21	[years]
CAPEX	483	460	437	[Euro/kg H_2]
O&M	1	1	1	[%]
Compressor				
Lifetime	10	10	10	[years]
CAPEX	2440	2440	2440	[Euro/kW]
O&M	4	4	4	[%]
Wind offshore				
Lifetime	25.7	27.0	28.4	[years]
CAPEX	2835	2700	2565	[Euro/kW_p]
O&M	2.4	2.4	2.4	[%]
Wind onshore				
Lifetime	25.7	27.0	28.4	[years]
CAPEX	1470	1400	1330	[Euro/kW_p]
O&M	2.4	2.4	2.4	[%]
Solar PV				
Lifetime	28.5	30	31.5	[years]
CAPEX	998	950	903	[Euro/kW_p]
O&M	2	2	2	[%]
Battery				
Depth of discharge	0.93	0.93	0.93	[-]
Roundtrip efficiency	0.91	0.91	0.91	[-]
CAPEX (battery pack)	189	180	171	[Euro/kWh]
Lifetime (battery pack)	12.4	13.0	13.7	[years]
CAPEX (power unit)	147	140	133	[Euro/kW]
Lifetime (power unit)	19	20	21	[years]
O&M	10	10	10	[Euro/kW/year]
Self disch. Rate	0.00054	0.00054	0.00054	[h^{-1}]
General				
System lifetime	20	20	20	[years]
Discount rate	0.08	0.07	0.05	[-]
Water desalination cost	0.018	0.018	0.018	[Euro/kg H_2]
Increase cost grid	n.a.	n.a.	n.a.	[$year^{-1}$]

E.2 Techno-economic scenarios for 2020

Table A4 shows the techno-economic parameters used for the sensitivity analysis for year 2020 (to show the error bars in Figure 4 in the manuscript). The pessimistic scenario is a scenario where the CAPEX is increased by 5% and the lifetimes are decreased by 5% of selected system components, compared to the figures provided in Table 1 (and the Baseline scenario) for 2020. While the optimistic scenario is a scenario where the CAPEX is decreased by 5%, and the lifetimes are increased by 5% of the selected system components. Further, the discount rates are varied between the scenarios.

Table A5: Life cycle results of all considered environmental impact categories, presented per kg H_2.

Location [km^2 land]	Configuration	Cobalt [kg]	GWP [kg CO_2-eq.]	Iridium [kg]	Land [m^2]	Lithium [kg]	Platinum [kg]	Silver [kg]	Tin [kg]	Titanium [kg]
Crete [8450 km^2]	Grid connected	2.16E-05	4.14E+01	6.68E-07	9.74E-03	3.07E-09	5.09E-08	9.18E-06	1.81E-05	2.24E-03
	Hybrid	1.66E-05	2.74E+01	6.96E-07	6.87E-03	2.60E-09	4.88E-08	6.40E-06	1.39E-05	2.21E-03
	Hybrid - Green	1.23E-05	4.51E+00	2.53E-06	2.67E-02	3.40E-09	1.50E-07	9.03E-06	1.28E-04	7.42E-03
	Autonomous	6.16E-04	3.97E+00	1.38E-06	4.80E-02	1.84E-03	1.04E-07	2.74E-05	3.46E-04	4.59E-03
	Autonomous - inj.	5.93E-04	3.95E+00	1.36E-06	4.78E-02	1.77E-03	1.02E-07	2.67E-05	3.40E-04	4.52E-03
Eigerøy [20 km^2]	Grid connected	1.85E-05	1.47E+00	6.68E-07	5.72E-03	1.64E-09	4.51E-08	3.89E-06	4.36E-06	1.98E-03
	Hybrid	1.59E-05	1.26E+00	6.68E-07	4.76E-03	1.57E-09	4.40E-08	3.26E-06	4.48E-06	1.97E-03
	Hybrid - Green	1.59E-05	1.26E+00	6.68E-07	4.76E-03	1.57E-09	4.40E-08	3.26E-06	4.48E-06	1.97E-03
	Autonomous	9.23E-04	4.30E+00	1.32E-06	3.60E-02	2.81E-03	1.10E-07	3.33E-05	3.57E-04	4.42E-03
	Autonomous - inj.	9.23E-04	4.30E+00	1.32E-06	3.60E-02	2.81E-03	1.10E-07	3.33E-05	3.57E-04	4.42E-03
Western Isles [3070 km^2]	Grid connected	2.08E-05	1.91E+01	6.68E-07	6.17E-02	3.23E-09	4.72E-08	7.38E-06	9.32E-06	2.35E-03
	Hybrid	1.39E-05	1.03E+01	6.69E-07	3.31E-02	2.34E-09	4.37E-08	4.30E-06	7.28E-06	2.15E-03
	Hybrid - Green	1.09E-05	4.40E+00	8.39E-07	1.36E-02	2.07E-09	5.17E-08	2.86E-06	7.07E-06	2.51E-03
	Autonomous	2.08E-04	2.18E+00	1.37E-06	1.56E-02	5.70E-04	8.82E-08	9.79E-06	1.08E-04	4.11E-03
	Autonomous - inj.	1.37E-04	2.07E+00	1.38E-06	1.45E-02	3.45E-04	8.67E-08	7.87E-06	8.73E-05	4.12E-03
Tenerife [2030 km^2]	Grid connected	2.15E-05	2.16E+01	6.68E-07	2.06E-02	3.84E-09	4.91E-08	6.62E-06	1.02E-05	2.41E-03
	Hybrid	1.51E-05	1.26E+01	6.68E-07	1.23E-02	2.80E-09	4.51E-08	4.17E-06	8.04E-06	2.20E-03
	Hybrid - Green	1.13E-05	4.40E+00	1.17E-06	1.74E-02	2.28E-09	7.15E-08	5.64E-06	6.84E-05	3.55E-03
	Autonomous	5.02E-04	3.20E+00	1.12E-06	3.78E-02	1.49E-03	8.35E-08	2.15E-05	2.75E-04	3.68E-03
	Autonomous - inj.	5.25E-04	3.25E+00	1.05E-06	3.83E-02	1.57E-03	8.04E-08	2.22E-05	2.82E-04	3.51E-03
Borkum [30 km^2]	Grid connected	2.37E-05	3.01E+01	6.68E-07	2.21E-02	4.29E-09	6.66E-08	1.21E-05	2.27E-05	3.66E-03
	Hybrid	1.97E-05	2.34E+01	6.68E-07	1.73E-02	3.60E-09	6.05E-08	9.55E-06	1.87E-05	3.27E-03
	Hybrid - Green	1.13E-05	4.40E+00	1.05E-06	1.25E-02	2.00E-09	6.57E-08	5.44E-06	4.96E-05	3.29E-03
	Autonomous	4.45E-04	3.78E+00	1.40E-06	4.00E-02	1.30E-03	9.98E-08	2.30E-05	2.70E-04	4.55E-03
	Autonomous - inj.	4.45E-04	3.78E+00	1.40E-06	4.00E-02	1.30E-03	9.98E-08	2.30E-05	2.70E-04	4.55E-03

F Life cycle results

The life cycle results are provided in Table A5. The maximum scores of environmental impact categories can be found in Table A5 as well, those are shaded in dark red.

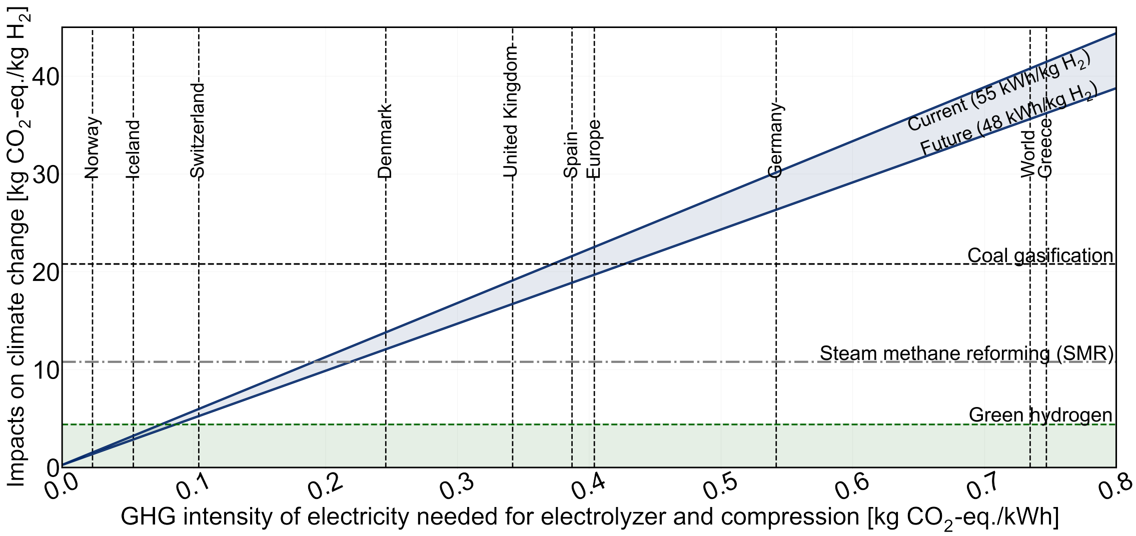

Figure A2: GHG emissions from grid-connected hydrogen production pathways using different grid electricity mixes for electricity in the electrolyzer and compressor on the x-axis [kg CO_2-eq./kg H_2]. The figures visualizes different scenarios regarding the efficiency of the PEM electrolyzer; a current scenario (55 kWh/kg H_2) and a future scenario (48 kWh/kg H_2).

Table A6: Electricity datasets used as vertical lines in Figure 6 in the main body of the article.

Electricity dataset	**ecoinvent reference product — name — location — unit —database**
Norway	electricity, low voltage — market for electricity, low voltage — NO — kilowatt hour — ecoinvent 3.7.1 cutoff
Iceland	electricity, low voltage — market for electricity, low voltage — IS — kilowatt hour — ecoinvent 3.7.1 cutoff
Switzerland	electricity, low voltage — market for electricity, low voltage — CH — kilowatt hour — ecoinvent 3.7.1 cutoff
Denmark	electricity, low voltage — market for electricity, low voltage — DK — kilowatt hour — ecoinvent 3.7.1 cutoff
United Kingdom	electricity, low voltage — market for electricity, low voltage — GB — kilowatt hour — ecoinvent 3.7.1 cutoff
Spain	electricity, low voltage — market for electricity, low voltage — ES — kilowatt hour — ecoinvent 3.7.1 cutoff
Europe	electricity, low voltage — market group for electricity, low voltage — ENTSO-E — kilowatt hour — ecoinvent 3.7.1 cutoff
Germany	electricity, low voltage — market for electricity, low voltage — DE — kilowatt hour — ecoinvent 3.7.1 cutoff
World	electricity, low voltage — market group for electricity, low voltage — GLO — kilowatt hour — ecoinvent 3.7.1 cutoff
Greece	electricity, low voltage — market for electricity, low voltage — GR — kilowatt hour — ecoinvent 3.7.1 cutoff

G Additional results

G.1 Grid-connected hydrogen production configurations

Figure A2 visualizes the (linear) dependence of the climate change impact on the GHG intensity of the (grid) electricity mix considering the efficiency of the PEM electrolyzer in two scenarios: the current efficiency (61% [55 kWh/kg H_2]) and a possible future efficiency in year 2040 (70% [48 kWh/kg H_2]). The shaded light blue area represents the climate change impact of electricity grid-coupled configurations between these two scenarios. Again, the colored dashed horizontal lines demonstrate the climate change impacts of coal gasification (in black), SMR (in gray),[35] and green hydrogen (in green).[7] The dashed vertical lines show the current GHG intensity of average country electricity mixes as comparison, details are provided in Table A6. More discussion is provided in Section 3.2.1 of the manuscript.

G.2 GHG credit for injection of electricity into the electricity network

Figure A3 is a bar plot showing GHG emissions for all considered configurations on different geographical locations on the x-axis. The y-axis illustrates the total score on GHG emissions. The different colored bar segments represent an activity with the size corresponding to its absolute climate change impact. The total impacts on climate change are provided above the bar segments for each configuration. As opposed to the analysis in the main body of the article, this figure includes a credit for GHG emissions. The GHG credit represents electricity injected into the grid and is accounted for using the GHG intensity of the electricity grid on average due to lack of data regarding the hourly marginal generation for the grid region of each of the analysed locations. It is worth noting that the total impact on climate change can therefore be negative. However, this does not mean negative emissions in terms of carbon removal but refers to GHG emissions that could be avoided compared to a reference system.[36]

In this situation, when considering a substantial credit for GHG emissions, Figure A3 demonstrates that the lowest impacts on climate change can be reached in configurations with significant injection of grid electricity for locations with GHG intensive national grid electricity networks, for example for the *autonomous - grid injection* configurations in Crete and Borkum. Interestingly, the configurations—*autonomous - grid injection* and *hybrid - green*—with low GHG intensive hydrogen production become even more beneficial in terms of GHG emissions, since these configurations generate excess renewable electricity since they are mostly based on renewable electricity sources. Excess renewable electricity can be injected into the electricity grid in this case, and could replace fossil fuel based grid electricity in some countries resulting in a substantial credit for GHG emissions.

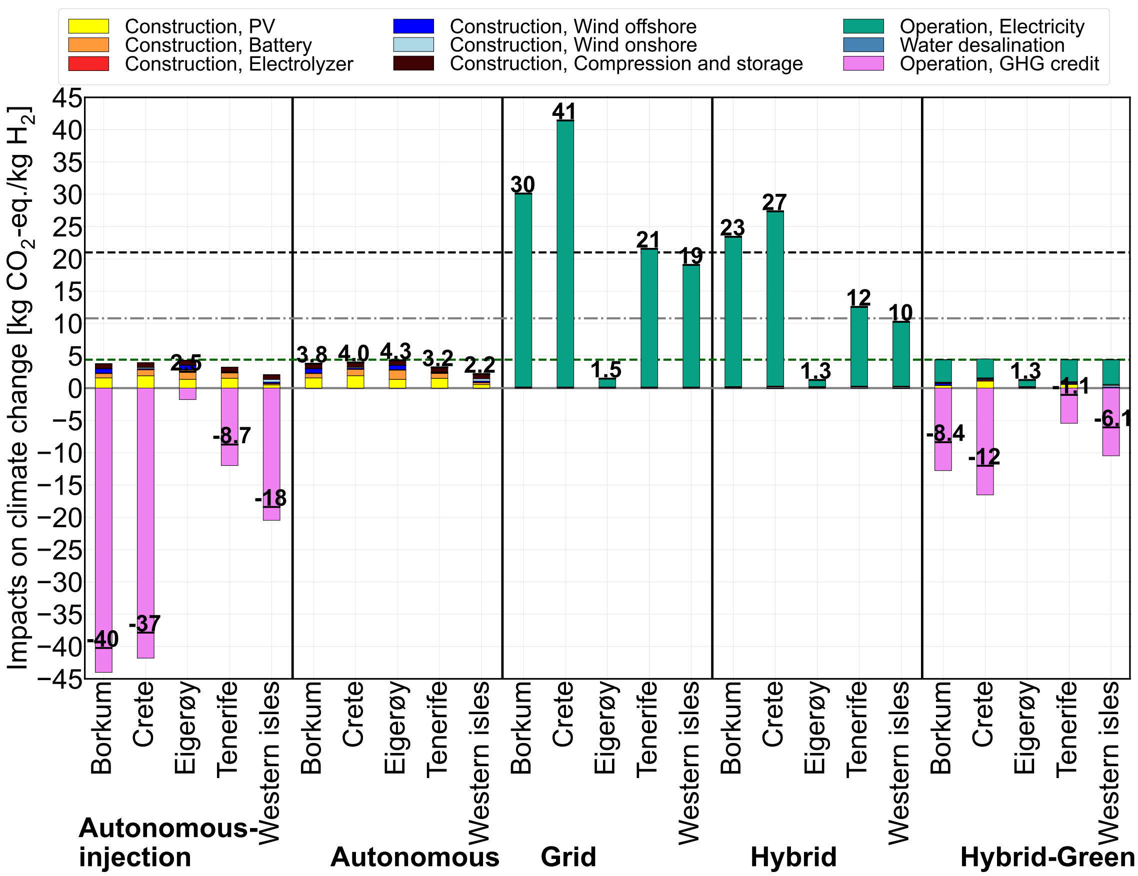

Figure A3: Impacts on climate change when considering a credit for injected GHG emissions into the electricity grid. The colored horizontal lines indicate the climate change impact of green hydrogen (green), gray hydrogen (in gray, dash-dotted), and black hydrogen (in black).[35] According to "CertifHy" renewable hydrogen should have a reduction of (at least) 60%—*i.e.,* lower than approximately 4.4 kg CO_2-eq./kg H_2—compared to hydrogen production *via* SMR of natural gas.[7,18]

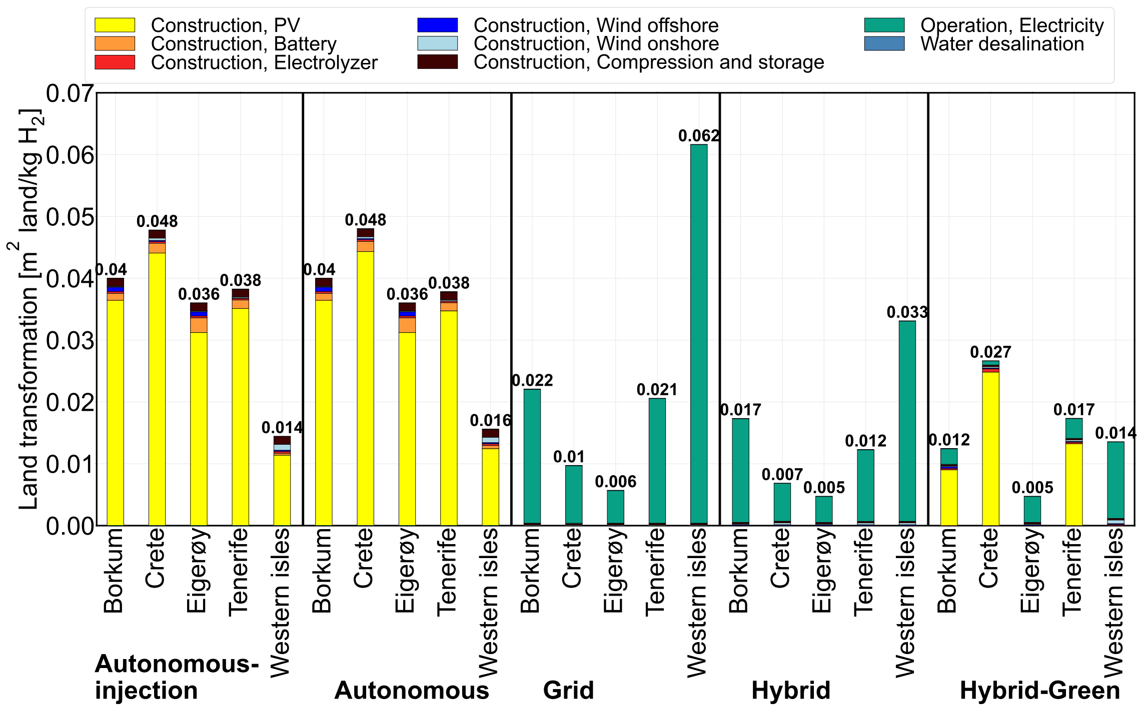

Figure A4: Contribution analysis of land transformation in m^2 per kg H_2 produced.

G.3 Land transformation

Further, Figure A4 shows a contribution analysis of land transformation for all configurations and case studies with the colors identifying specific processes from a life cycle perspective. The total land transformation is provided above the bars (in m^2 per kg H_2).

Figure A4 shows that grid electricity (for grid-connected and hybrid configurations) and solar PV systems (for autonomous configurations) are the main contributors to land transformation. Hydrogen production configurations with a large solar PV capacity installed can exhibit large direct land transformation due to the area requirement of ground-mounted PV installations. More discussion regarding the land transformation of ground-mounted PV installations is provided in Ref.[37] Land transformation due to grid electricity can be considered as indirect transformation, since the land is transformed in other places to (for example) harvest biomass as in the case of Western Isles (UK). Power generation related land transformation is in general comparatively high in countries with substantial shares of non-residual biomass for electricity production, such as in the UK.

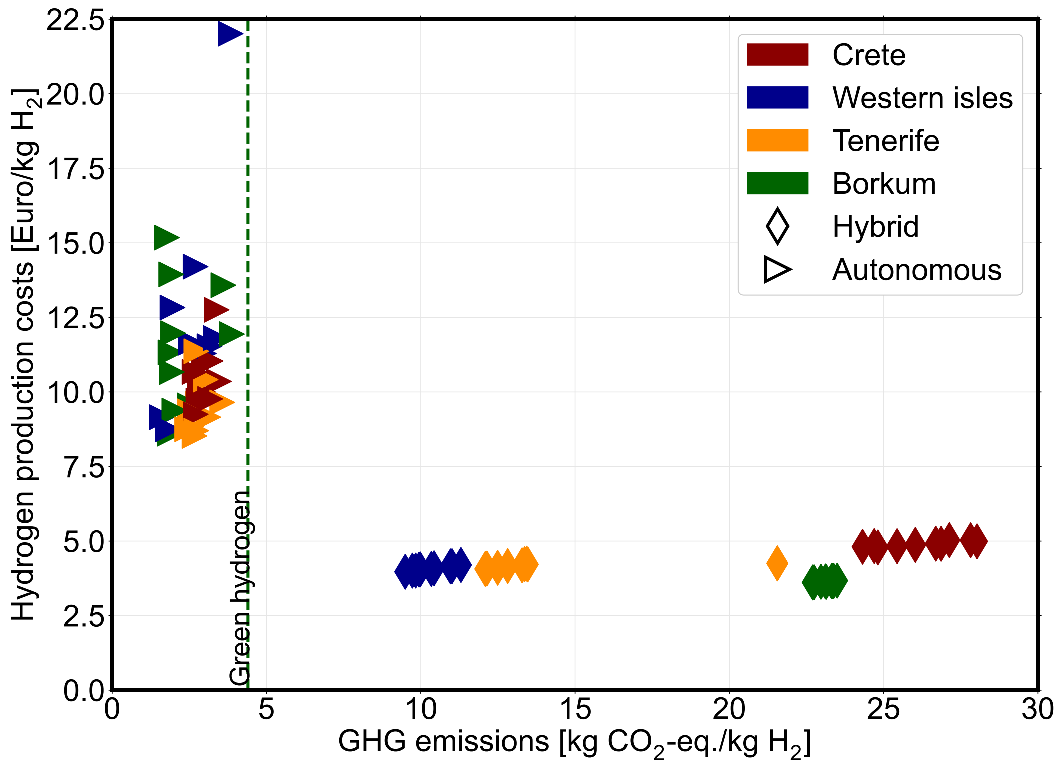

Figure A5: Results from the sensitivity analysis on different input data regarding weather conditions (windspeed, solar irradiation, and temperature) applying a cost optimization. One outlier (autonomous for Western Isles in 2008) is excluded in this figure as a result of missing/erroneous input data leading to extremely high costs and/or environmental burdens. Further, non-TMY data is not available for Eigerøy, and this geographical location has therefore been excluded from this figure.

G.4 Sensitivity: weather data inputs

Figure A5 illustrates the sensitivity analysis using different hourly weather data inputs for years 2007-2016; this means ten additional results for each configuration and geographical location. The results of these simulations are presented for life cycle GHG emissions on the x-axis and hydrogen production costs on the y-axis. The locations are visualized with different colors, while the configurations are illustrated with different markers. Grid-connected configurations are not included in this figure, since meteorological conditions do not directly affect grid-connected system configurations in our simulations. More discussion is provided in Section 3.3.3 of the manuscript.

G.5 Weekly system operations

Eigerøy (Norway) and Tenerife (Spain) are selected as case studies since they represent a colder and warmer climate, respectively, and therefore have, among others, different energy generation profiles from wind and PV solar.

G.5.1 Eigerøy

Figure A6 and Figure A7 illustrate the system operation of a winter week in Eigerøy (Norway) for the *autonomous* and *autonomous - grid injection* configurations, respectively. Further, Figure A8 and Figure A9 illustrate the system operation of a summer week in Eigerøy (Norway) for the *autonomous* and *autonomous - grid injection* configurations, respectively. It is worth noting that PV solar, onshore wind as well as offshore wind are installed as electricity generators for both configurations for these specific cases.

The first subplot, to the top left, shows the renewable electricity generation during this winter week. The second subplot shows, besides the actual renewable electricity generation (represented by positive values), the curtailment of renewable electricity (represented as negative values). The third subplot shows the charging (negative values) and discharging (positive values) of the battery (in case installed). The fourth subplot represents the state of charge (SoC) of the battery system, respecting the minimum and maximum SoC. The fifth subplot presents the electricity consumption of the electrolyzer, required to generate hydrogen. And lastly, the sixth subplot shows possible remuneration of grid electricity injection, which does not apply for the fully *autonomous* configuration since it is disconnected from the electricity grid. It is, however, worth noting that a remuneration of grid electricity is available for the *autonomous - grid injection* configuration, see for example Figure A7. In this situation, excess renewable electricity can be injected into the electricity grid, which can be seen in the second subplot.

The winter week in Eigerøy (Norway) for the *autonomous* configuration (Figure A6) shows that on days with an excess of renewable electricity—for example on the 6^{th}, 8^{th} or 9^{th} of February—a significant amount of renewable electricity is curtailed. Further, the battery is not intensively used as it cannot be used to first store and subsequently sell electricity to the electricity network. In this situation, it is mainly used to store electricity to be used on days when there is a shortage of renewable electricity generation. On the contrary, the winter week in Eigerøy (Norway) in Figure A7 for the *autonomous - grid injection* configuration shows that there is no curtailment of electricity. Instead, excess electricity from renewables is sold and injected into the electricity grid, to generate revenue. Further, the battery is slightly more used to enable the selling of—otherwise curtailed—excess electricity to the electricity grid.

The summer week in Eigerøy (Norway) in Figure A8 for the *autonomous* configuration shows a similar pattern; a significant amount of electricity is curtailed. On the contrary, the summer week in Eigerøy (Norway) in Figure A9 for the *autonomous - grid injection* configuration shows much less curtailment of electricity.

Again, excess electricity from renewables can be sold and injected into the electricity grid, to generate additional revenue from excess electricity generation. Further, the battery is more intensively used to enable selling of—otherwise curtailed—excess electricity to the electricity network.

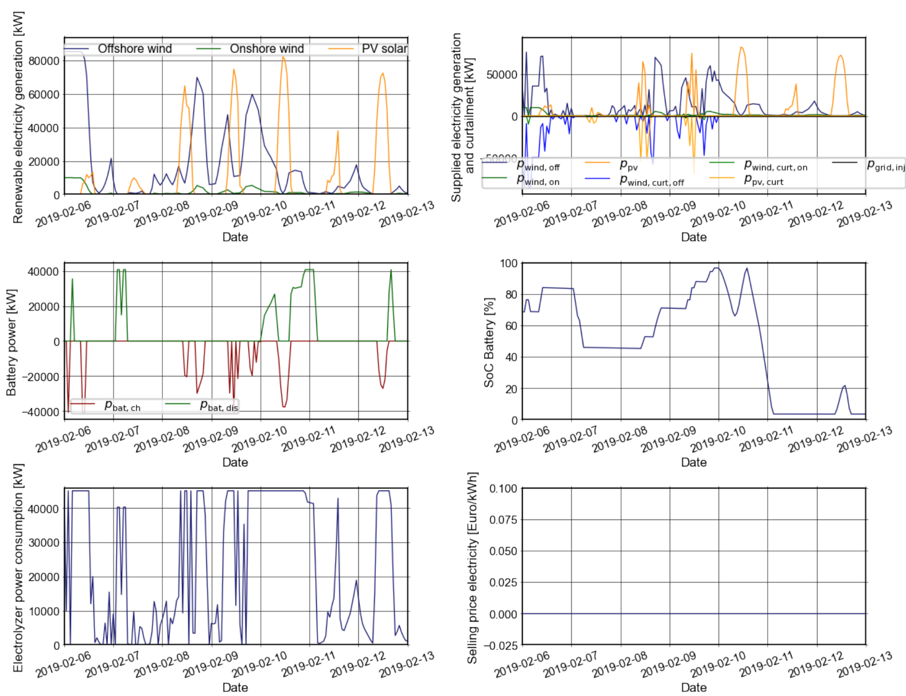

Figure A6: System operation during a winter week for the *autonomous* configuration in Eigerøy.

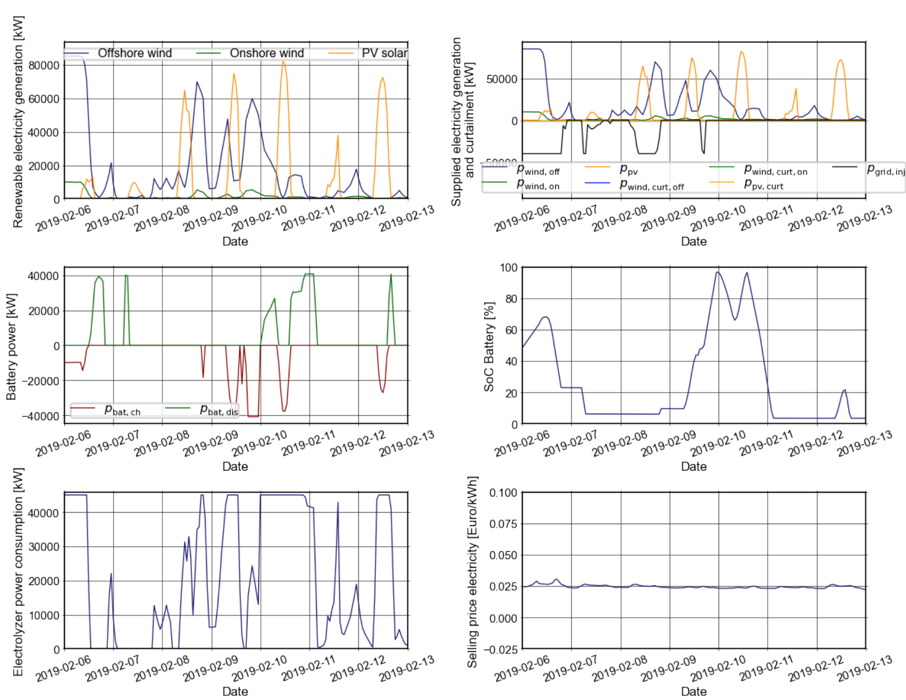

Figure A7: System operation during a winter week for the *autonomous - grid injection* configuration in Eigerøy.

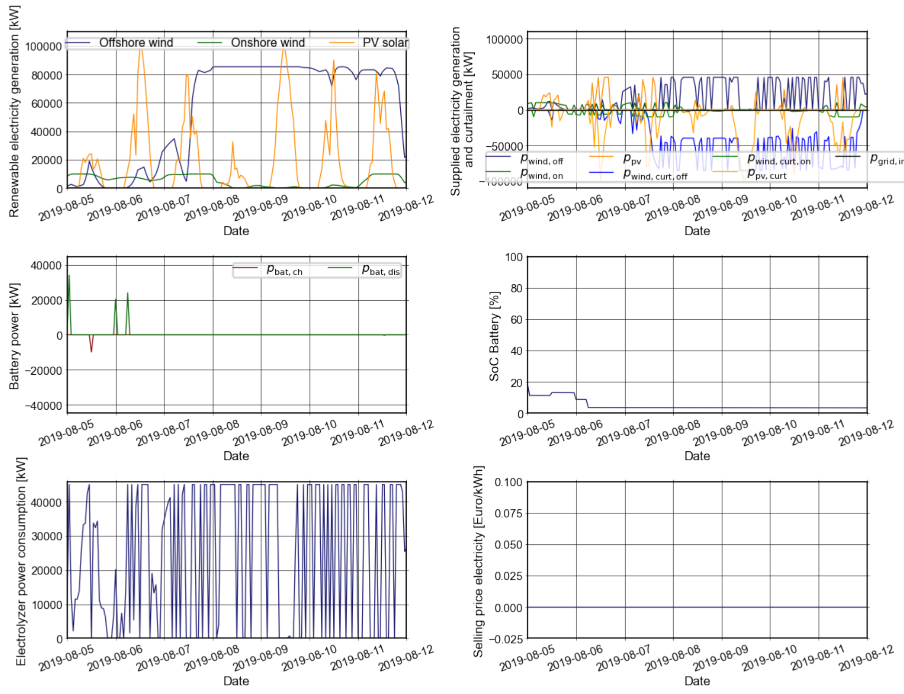

Figure A8: System operation during a summer week for the *autonomous* configuration in Eigerøy.

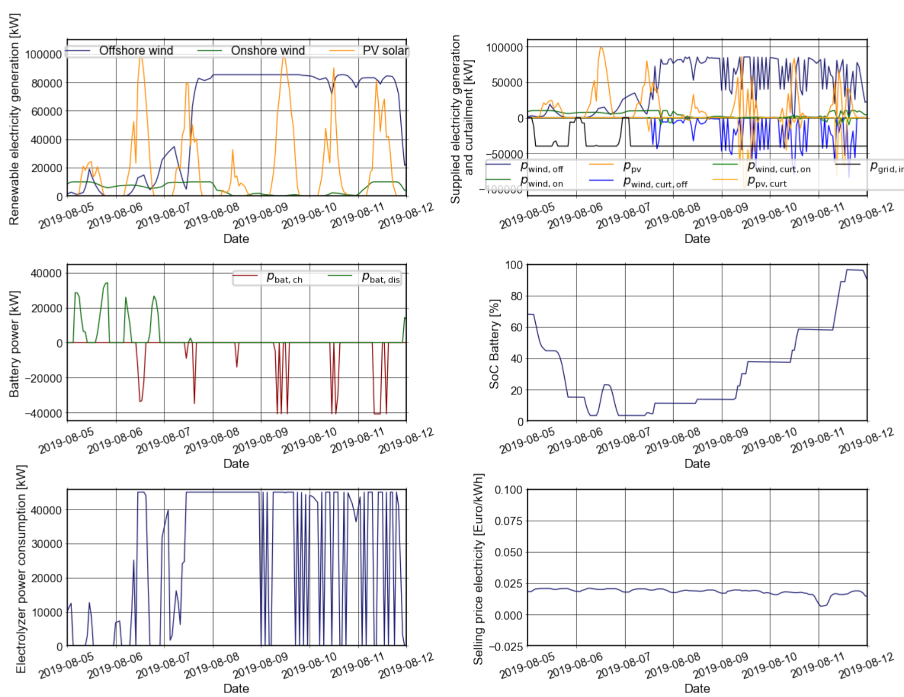

Figure A9: System operation during a summer week for the *autonomous - grid injection* configuration in Eigerøy.

G.5.2 Tenerife

Figure A10 and Figure A11 illustrate the system operation of a winter week in Tenerife (Spain) for the *autonomous* and *autonomous - grid injection* configurations, respectively. Figure A12 and Figure A13 illustrate the system operation of a summer week in Tenerife (Spain) for the *autonomous* and *autonomous - grid injection* configurations, respectively. More explanation regarding the subplots is provided in previous Section G.5.1.

It is worth noting that only a very small capacity of offshore wind is installed on Tenerife, mainly onshore wind and PV solar, mainly due to lower costs. The winter week in Tenerife (Figure A10) for the *autonomous* configuration demonstrates that also during winter there is excess solar PV generation and therefore most of the excess electricity is curtailed. On the contrary, the winter week in Tenerife (Figure A10) of the *autonomous - grid injection* configuration shows that no excess renewable electricity generation is curtailed; excess electricity is injected into the electricity network to generate additional revenue. Further, the battery is more intensively used (around one full battery cycle per day) to store excess electricity and to sell it during timeslots with higher selling prices for electricity, since the last subplot shows that the variability of electricity prices has been significant during this winter week.

The summer week in Tenerife in Figure A12 and Figure A13 illustrates a high availability of solar PV generation. Again, more curtailment in the fully *autonomous* configuration compared to the *autonomous - grid injection* configuration.

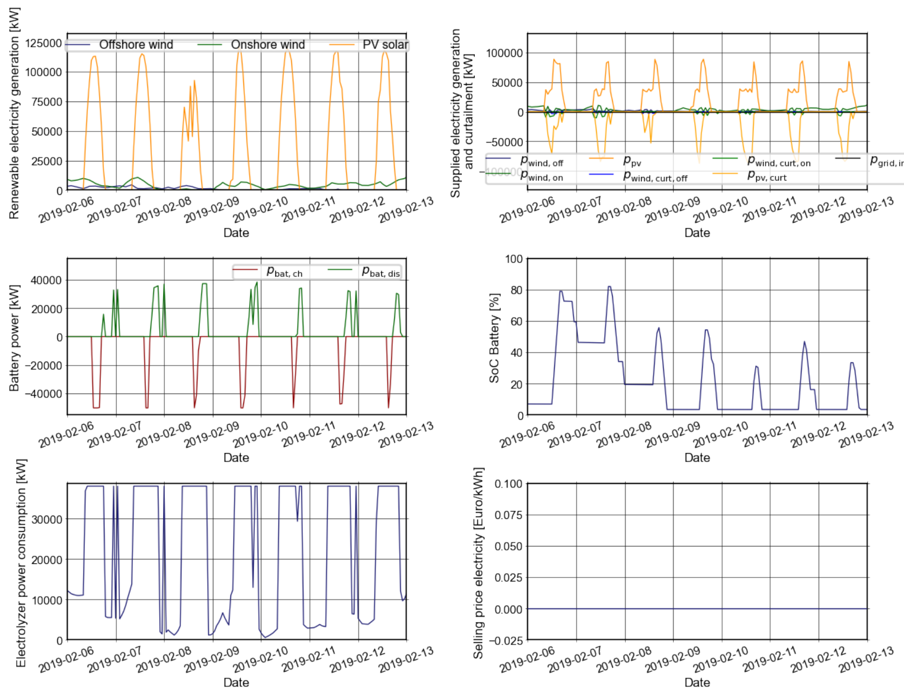

Figure A10: System operation during a winter week for the *autonomous* configuration in Tenerife.

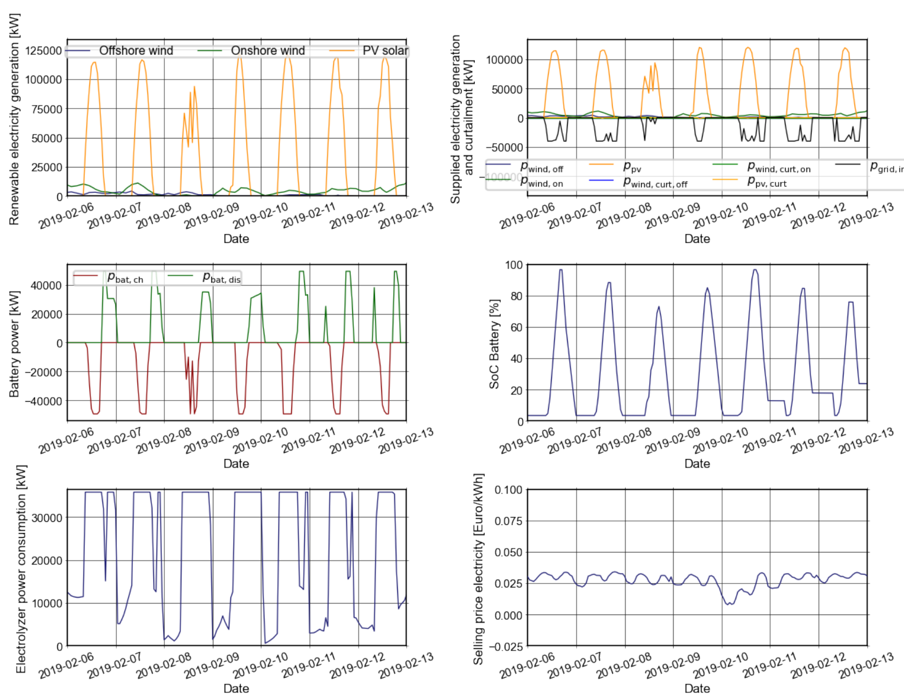

Figure A11: System operation during a winter week for the *autonomous - grid injection* configuration in Tenerife.

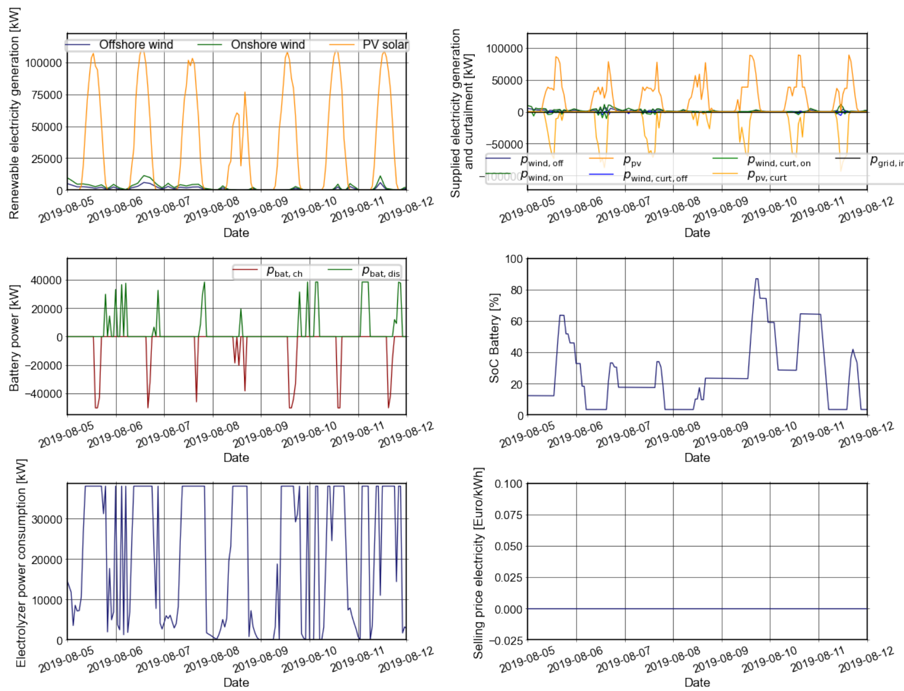

Figure A12: System operation during a summer week for the *autonomous* configuration in Tenerife.

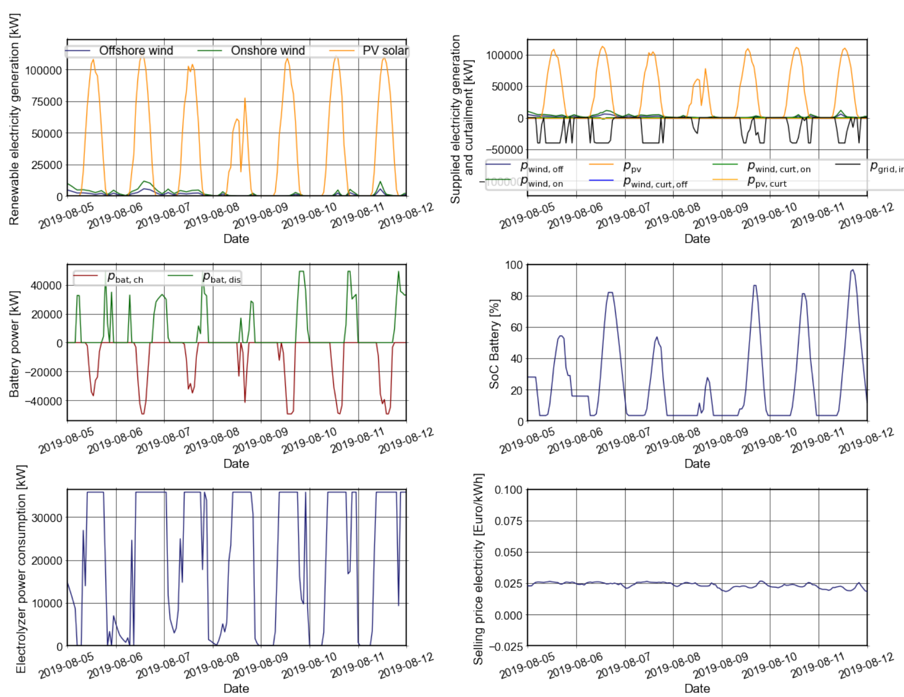

Figure A13: System operation during a summer week for the *autonomous - grid injection* configuration in Tenerife.

Table A7: Initial investments (at t=0) and annualized costs for operation, replacement, O&M, and investments for reference year 2020. Further, the total annualized costs and hydrogen production costs are provided per island and configuration.

Location	Configuration	Initial investments [million €]	Investments [million €/year]	Operation [million €/year]	Replacement [million €/year]	O&M [million €/year]	Total annualized costs [million €/year]	Hydrogen costs [Euro/kg H_2]
Borkum	Autonomous - inj.	507.3	47.9	-5.6	2.4	10.2	54.9	15.0
	Autonomous	500.1	47.2	0.1	2.5	10.2	59.9	16.4
	Grid connected	36.8	3.5	7.8	1.7	0.5	13.5	3.7
	Hybrid	50.8	4.8	6.1	1.6	0.9	13.4	3.7
	Hybrid - Green	192.3	18.2	-0.8	1.9	4.1	23.3	6.4
Crete	Autonomous - inj.	402.9	38.0	-6.5	3.2	7.5	42.2	11.6
	Autonomous	393.2	37.1	0.1	3.4	7.4	47.9	13.1
	Grid connected	36.8	3.5	13.1	1.7	0.5	18.8	5.1
	Hybrid	71.4	6.7	8.5	1.6	1.4	18.2	5.0
	Hybrid - Green	263.1	24.8	-1.4	5.6	5.3	34.4	9.4
Eigerøy	Autonomous - inj.	533.8	50.4	-5.3	3.4	9.8	58.3	16.0
	Autonomous	526.6	49.7	0.1	3.4	9.8	63.0	17.2
	Grid connected	36.8	3.5	8.1	1.7	0.5	13.8	3.8
	Hybrid	50.8	4.8	6.5	1.6	0.9	13.8	3.8
	Hybrid - Green	50.8	4.8	6.5	1.6	0.9	13.8	3.8
Tenerife	Autonomous - inj.	293.2	27.7	-2.6	2.7	5.0	32.8	9.0
	Autonomous	284.7	26.9	0.1	2.9	5.0	34.9	9.6
	Grid connected	36.8	3.5	9.8	1.7	0.5	15.5	4.3
	Hybrid	69.0	6.5	5.8	1.5	1.3	15.1	4.1
	Hybrid - Green	168.4	15.9	0.4	2.4	3.4	22.1	6.1
Western Isles	Autonomous - inj.	303.0	28.6	-5.4	2.7	6.2	32.2	8.8
	Autonomous	295.3	27.9	0.1	2.9	6.1	36.9	10.1
	Grid connected	36.8	3.5	10.2	1.7	0.5	15.8	4.3
	Hybrid	69.5	6.6	5.4	1.5	1.3	14.8	4.1
	Hybrid - Green	154.7	14.6	-0.8	1.6	3.4	18.7	5.1

G.6 Cost result table

Table A7 shows the annualized costs regarding operation, replacement, O&M, and investments for reference year 2020 (the baseline scenario). Further, total annualized costs and the costs per kilogram hydrogen are provided.

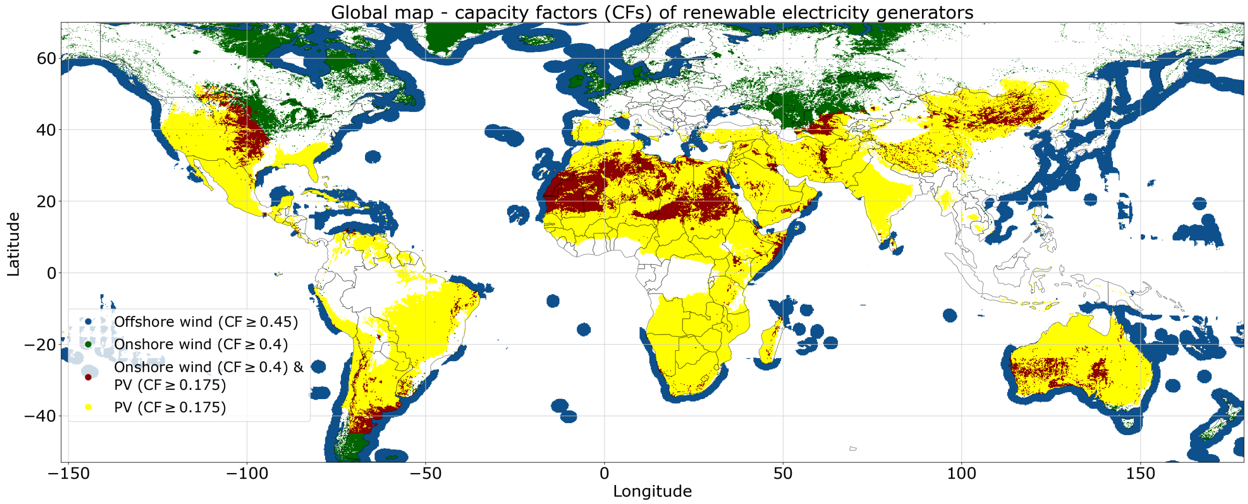

Figure A14: Global map—capacity factors of renewable electricity generators. CF = capacity factor.

H Global map: capacity factors of renewable electricity generators

Figure A14 is a global map illustrating potentially favorable locations for green hydrogen production based on the capacity factor (CF) of three renewable electricity generators; onshore wind, offshore wind, and solar PV.

Solar PV data is obtained from the "Global Solar Atlas 2.0, a free, web-based application is developed and operated by the company Solargis s.r.o. on behalf of the World Bank Group, utilizing Solargis data, with funding provided by the Energy Sector Management Assistance Program (ESMAP). For additional information: https://globalsolaratlas.info".[38]

Further, wind data is obtained from "Global Wind Atlas 3.0, a free, web-based application developed, owned and operated by the Technical University of Denmark (DTU). The Global Wind Atlas 3.0 is released in partnership with the World Bank Group, utilizing data provided by Vortex, using funding provided by the Energy Sector Management Assistance Program (ESMAP). For additional information: https://globalwindatlas.info".[39,40]

For onshore wind, we use class "IEC1", since this refers to wind turbines with a lower rotor diameter compared to, for example, class "IEC3" (more wind power output), which has been selected for offshore wind capacity factors.[40] It is worth noting that offshore wind potentials are covered up to 200 km from the shoreline.[39]

References

[1] R. Baldick, *Applied optimization: Formulation and algorithms for engineering systems*, Cambridge University Press, 2006, vol. 9780521855, pp. 1–768.

[2] P. Gabrielli, M. Gazzani, E. Martelli and M. Mazzotti, *Applied Energy*, 2018, **219**, 408 – 424.

[3] L. Gurobi Optimization, *Gurobi Optimizer Reference Manual*, 2021, `http://www.gurobi.com`.

[4] H. Energy, *Homer Energy—Annualized Costs*, 2022, `https://www.homerenergy.com/products/pro/docs/latest/annualized_cost.html`, Accessed on Thursday, January 13, 2022.

[5] M. Ehrgott, *Multicriteria optimization*, Springer Science & Business Media, 2005, vol. 491.

[6] K. Chircop and D. Zammit-Mangion, *Journal of Mechanics Engineering and Automation*, 2013, **3**, 279–289.

[7] CertifHy, *CertifHy - Developing a European Framework for the generation of guarantees of origin for green hydrogen*, 2016, `https://www.certifhy.eu/images/media/files/CertifHy_-_definition_outcome_and_scope_LCA_analysis.pdf`, Accessed on Tuesday, September 31, 2021.

[8] B. Zakeri and S. Syri, *Renewable and sustainable energy reviews*, 2015, **42**, 569–596.

[9] A. Rodrigues, D. Machado and T. Dentinho, *Sustainability*, 2017, **9**, 1276.

[10] F. Glover, *Management Science*, 1975, **22**, 455–460.

[11] T. Terlouw, X. Zhang, C. Bauer and T. Alskaif, *Journal of Cleaner Production*, 2019, **221**, 667–677.

[12] T. S. Schmidt, M. Beuse, X. Zhang, B. Steffen, S. F. Schneider, A. Pena-Bello, C. Bauer and D. Parra, *Environmental Science and Technology*, 2019, **53**, 3379–3390.

[13] D. Parra and M. K. Patel, *International Journal of Hydrogen Energy*, 2016, **41**, 3748–3761.

[14] P. Gabrielli, M. Gazzani and M. Mazzotti, *Applied Energy*, 2018, **221**, 557–575.

[15] B. Xu, A. Oudalov, A. Ulbig, G. Andersson and D. S. Kirschen, *IEEE Transactions on Smart Grid*, 2016, **9**, 1131–1140.

[16] F. Khatib, T. Wilberforce, O. Ijaodola, E. Ogungbemi, Z. El-Hassan, A. Durrant, J. Thompson and A. Olabi, *Renewable and Sustainable Energy Reviews*, 2019, **111**, 1–14.

[17] K. Bareiß, C. de la Rua, M. Möckl and T. Hamacher, *Applied Energy*, 2019, **237**, 862–872.

[18] G. Palmer, A. Roberts, A. Hoadley, R. Dargaville and D. Honnery, *Energy & Environmental Science*, 2021, **14**, 5113–5131.

[19] R. Frischknecht, P. Stolz, L. Krebs, M. de Wild-Scholten, P. Sinha, V. Fthenakis, H. C. Kim, M. Raugei and M. Stucki, *Life Cycle Inventories and Life Cycle Assessment of Photovoltaic Systems, International Energy Agency (IEA) PVPS Task 12, Report T12-19:2020*, 2020.

[20] ecoinvent, *ecoinvent 3.7.1.*, 2021, https://ecoinvent.org/the-ecoinvent-database/data-releases/ecoinvent-3-7-1/, Accessed on Sunday, October 31, 2021.

[21] C. Bauer, T. Heck, S. Schneider, H. Sanjaykumar, T. Terlouw, K. Treyer and X. Zhang, *Electricity storage and hydrogen: Technologies, costs and environmental burdens*, Psi, paul scherrer institut technical report, 2021.

[22] R. Sacchi, T. Terlouw, K. Siala, A. Dirnaichner, C. Bauer, B. Cox, C. Mutel, V. Daioglou and G. Luderer, *Renewable and Sustainable Energy Reviews*, 2022, **160**, 112311.

[23] M. Armand, P. Axmann, D. Bresser, M. Copley, K. Edström, C. Ekberg, D. Guyomard, B. Lestriez, P. Novák, M. Petranikova *et al.*, *Journal of Power Sources*, 2020, **479**, 228708.

[24] ENTSOE, *ENTSO-E Transparency Platform*, 2021, https://transparency.entsoe.eu/dashboard/show.

[25] M. Uche-Soria and C. Rodríguez-Monroy, *Sustainability (Switzerland)*, 2018, 2572.

[26] Reuters, *Greek undersea cable links Crete island to the Peloponnese*, 2021, https://www.reuters.com/article/greece-power-link-idUSL5N2OF06V.

[27] S. Suárez García, *Perspectives of marine renewable energies in the Canary islands*, 2019, https://www.een-canarias.org/wp-content/uploads/2019/05/1.-Perspectivas-de-las-EERR-marinas-en-Canarias_Salvador-Su%C3%A1rez.pdf.

[28] T. Nguyen, Z. Abdin, T. Holm and W. Mérida, *Energy Conversion and Management*, 2019, **200**, 112108.

[29] EWEA, *EWEA position paper on network tariffs and grid connection regimes (revisited). European Wind Energy Association (EWEA). March 2016.*, 2016.

[30] T. Huld, R. Müller and A. Gambardella, *Solar Energy*, 2012, **86**, 1803–1815.

[31] W. F. Holmgren, C. W. Hansen and M. A. Mikofski, *Journal of Open Source Software*, 2018, **3**, 884.

[32] W. Holmgren, Calama-Consulting, C. Hansen, K. Anderson, M. Mikofski, A. Lorenzo, U. Krien, bmu, C. Stark, DaCoEx, A. Driesse, A. R. Jensen, M. S. de León Peque, konstant_t, mayudong, Heliolytics, E. Miller, M. A. Anoma, V. Guo, L. Boeman, J. Stein, W. Vining, jforbess, T. Lunel, A. Morgan, J. Ranalli, C. Leroy, A. M. R, JPalakapillyKWH and J. Dollinger, *pvlib/pvlib-python: v0.9.0*, 2021, `https://doi.org/10.5281/zenodo.5366883`.

[33] S. Haas, U. Krien, B. Schachler, S. Bot, kyri petrou, V. Zeli, K. Shivam and S. Bosch, *wind-python/windpowerlib: Silent Improvements*, 2021.

[34] Meteostat, *Meteostat Python Package*, 2021, `https://github.com/meteostat/meteostat-python`.

[35] T. Longden, F. J. Beck, F. Jotzo, R. Andrews and M. Prasad, *Applied Energy*, 2021, **266**, 118145.

[36] T. Terlouw, C. Bauer, L. Rosa and M. Mazzotti, *Energy Environ. Sci.*, 2021, **14**, 1701–1721.

[37] T. Terlouw, K. Treyer, C. Bauer and M. Mazzotti, *Environmental Science & Technology*, 2021, **55**, 11397–11411.

[38] Global Solar Atlas 2.0, *Global Solar Atlas 2.0*, 2022, `https://globalsolaratlas.info`, Accessed on Thursday, January 13, 2022.

[39] Global Wind Atlas 3.0, *Global Wind Atlas 3.0*, 2022, `https://globalwindatlas.info/`, Accessed on Thursday, January 13, 2022.

[40] N. Davis, J. Badger, A. N. Hahmann, B. O. Hansen, B. T. Olsen, N. G. Mortensen, D. Heathfield, M. Onninen, G. Lizcano and O. Lacave, *Global Wind Atlas v3*, 2019, `https://data.dtu.dk/articles/dataset/Global_Wind_Atlas_v3/9420803`.